NEUROSCIENCE

Complementary corticostriatal circuits orchestrate action repetition and switching

Baibing Zhang[1,2], Claire E. Geddes[2], Xin Jin[1,3]*

Action sequencing is fundamental to behavior. A critical decision for survival and reproduction is whether to repeat a current action or switch to a different one. However, the neural mechanisms governing action repetition and switching remain largely unknown. In mice trained to perform heterogeneous action sequences, we found that the M1-DLS circuit regulates action repetition, while the PrL-DMS pathway controls action switching. These distinct functions arise from preferential innervation of striatal D1-SPNs by M1 and D2-SPNs by PrL, respectively. In a Shank3 knockout mouse model of ASD, the D1/D2 innervation ratio in the PrL-DMS pathway was reversed, leading to impaired action switching and repetitive behaviors. Genetic restoration of Shank3 in the DMS rescued both physiological and behavioral deficits. These findings reveal how the brain orchestrates action sequencing in health and disease.

INTRODUCTION

Goal-directed behaviors, no matter how intricate they are, can be organized and chunked into fundamental units termed "action sequence" (*1*–*3*). At each given moment during the execution of an action sequence, the brain has to decide whether to repeat the same current action or switch to a different one, a fundamental problem in action selection (*2*–*4*). Knowing when to repeat or switch actions is thus critical for animals' survival and reproduction. Across the animal kingdom, action sequences form the foundation of diverse motor repertoires (*2*, *3*, *5*–*7*), with their impairment associated with various neurological and psychiatric disorders in humans, including Parkinson's disease (PD), Huntington's disease (HD), obsessive-compulsive disorder (OCD), and autism spectrum disorder (ASD) (*8*–*12*). Specifically, pathological repetitive behaviors are typically observed in conditions such as HD, OCD, and ASD (*13*–*17*), while action initiation is deficient in PD (*18*, *19*). Fundamentally, these seemingly markedly different disorders consist of a common problem of motor repetition and switching dysfunction during action sequencing (*3*, *20*). Despite the apparent behavioral significance, however, the neural circuit mechanisms underlying action repetition and switching in normal brains are poorly understood. Furthermore, it is unclear how the proper interplay between action repetition and switching is compromised in various diseases, posing a mechanistic burden for developing effective therapeutic interventions for these conditions (*15*, *21*–*23*).

The basal ganglia are thought to be critically involved in action selection and action sequencing (*3*, *4*, *6*, *7*), which are implemented primarily through its two major neural pathways (direct and indirect) originating from striatal D1- and D2-expressing spiny projection neurons (D1- and D2-SPNs), respectively (*20*, *24*–*27*). It has been previously found in mice that after learning a heterogeneous sequence, optogenetic activation of striatal D1-SPNs facilitates action repetition, while the activation of striatal D2-SPNs triggers behavioral switching (*20*). Anatomically, the striatum receives excitatory inputs from the cerebral cortex and thalamus (*28*, *29*). Accumulating evidence suggests that the corticostriatal synaptic transmission goes awry in disorders such as OCD (*30*–*32*) and ASD (*33*), implying that altered cortical projections onto striatal D1- and D2-SPNs might underlie some key behavioral symptoms in these conditions (*34*). However, which cortical areas are involved in action sequencing and how they control striatal D1- versus D2-SPNs to mediate action repetition and switching in health and disease remain critical yet unresolved questions.

In this study, we trained mice to perform a heterogeneous action sequence task (*20*) that incorporates both motor repetition and switching to dissect the corticostriatal mechanism underlying action sequencing behavior. We first identified the crucial roles of the primary motor cortex (M1) and prelimbic cortex (PrL) in the performance of learned sequence behavior by pharmacological inactivation and optogenetic silencing. In vivo neuronal recordings revealed M1 and PrL exhibit different sequence-related neuronal activity, implying their distinct functions in controlling different hierarchical levels of action sequence. Optogenetic activation of M1 to dorsolateral striatum (DLS) pathway, whether by stimulating on the DLS-projecting M1 neuronal soma or M1 terminals in DLS, facilitated the repetition of ongoing actions. In contrast, the optogenetic activation of PrL to dorsomedial striatum (DMS) pathway, whether by stimulating the DMS-projecting PrL neuronal soma or PrL terminals in DMS, triggers action switching. Further patch-clamp recordings from brain slices determined these functional specificities stem from the preferential innervations of M1 to D1-SPNs and PrL to D2-SPNs, respectively. In addition, it was found that activation of PrL-DMS pathway caused strong suppression of M1 neurons in vivo, suggesting a unidirectional inhibition from the action switching to action repetition circuit. These findings establish the neural logic underlying action selection and unveil the interaction between action repetition and switching circuits to the control of action sequencing.

We further investigated the neural circuits underlying action repetition and switching in *Shank3* knockout (KO) mice, a genetic variant linked to ASD exhibiting repetitive behavior (*33*). When trained with the LLRR task, the *Shank3* KOs showed marked deficits in sequence learning and performed notably more repetitive actions compared to their littermate controls. Slice recordings revealed a

[1]New Cornerstone Science Laboratory, Center for Motor Control and Disease, Key Laboratory of Brain Functional Genomics, East China Normal University, 3663 North Zhongshan Road, Shanghai 200062, China. [2]Molecular Neurobiology Laboratory, The Salk Institute for Biological Studies, 10010 North Torrey Pines Road, La Jolla, CA 92037, USA. [3]NYU–ECNU Institute of Brain and Cognitive Science, New York University Shanghai, 3663 North Zhongshan Road, Shanghai 200062, China.
*Corresponding author. Email: xjin@bio.ecnu.edu.cn

reversal in the D1/D2 ratio in the PrL-DMS projections of these mutants. Consequently, the optogenetic stimulation of the PrL-DMS pathway in the *Shank3* KO mice failed to trigger action switching and instead induced action repetition. In addition, the modulation effect of the PrL-DMS pathway on M1 shifted from inhibitory to excitatory in the mutants, further enhancing the action repetition pathway, thereby contributing to the repetitive behaviors. Notably, the viral restoration of *Shank3* in DMS, but not DLS, is sufficient to correct the reversed D1/D2 ratio in the PrL-DMS circuit and rescued action switching during sequence behavior, leading to the recovery of sequential behavior and normalization of grooming. These results have important implications for understanding the cortico-basal ganglia mechanism underlying action selection, including the dynamic interplay between action repetition and switching in health and disease.

RESULTS

Both M1 and PrL are involved in execution of learned action sequence

To investigate the corticostriatal mechanism underlying action selection, we trained mice to perform a left-left-right-right (LLRR) "Penguin Dance" action sequence task, which includes both action repetition and action switching (*20*). The experimental setup included a training chamber equipped with left and right levers and a reward-delivering magazine positioned in the opposite side (Fig. 1A). A food pellet reward was delivered whenever a LLRR lever press sequence is performed by mice (see Materials and Methods). This "LLRR" action sequence is hierarchically organized and includes both the repetition of the same action (LL and RR) and switching between different actions (L-R) (Fig. 1B). After 21 days of LLRR training, mice significantly increased the pattern of LLRR sequence and achieved a performance efficiency of more than 40% (Fig. 1C, effect of training: for M1 group, $n = 7$, $F_{20,120} = 2.118$, $P = 0.0069$; for PrL group, $n = 7$, $F_{20,120} = 2.759$, $P = 0.0003$; fig. S1, A to F). It has been previously shown that the dorsal striatum, including both D1- and D2-SPNs, are necessary for the execution of learned LLRR sequence (*20*). The striatum receives topographic glutamatergic inputs from the cerebral cortex, with M1 projecting to the DLS and PrL primarily targeting the DMS, respectively (*35*, *36*). To determine the roles of cortical regions in action sequence execution, we injected muscimol bilaterally to inactivate M1 or PrL in the trained mice when they were performing the LLRR task (see Materials and Methods). Notably, muscimol infusion into either M1 (Fig. 1; $n = 7$, efficiency of pre: 50.3 ± 1.8%; muscimol: 35.3 ± 3.4%; post: 49.0 ± 2.3%, paired *t* test between pre and muscimol: $P = 0.003$; between muscimol and post: $P = 0.002$; fig. S1, G to I) or PrL (Fig. 1E; $n = 7$, efficiency of pre: 46.2 ± 3.2%; muscimol: 20.3 ± 2.8%; post: 43.2 ± 3.7%, paired *t* test between pre and muscimol: $P = 0.002$; between muscimol and post: $P = 0.008$; fig. S1, J to L) significantly reduced the sequence performance efficiency compared with the pre- and post-control of saline injection in the same animals. These results suggest that both M1 and PrL are involved in the execution of learned action sequence. Furthermore, we calculated the repetition versus switching ratio, defined as the percentage of repetition lever presses (LL or RR) divided by the percentage of switching lever presses (LR or RL) within a session for both groups under three different conditions. We found that inactivation of M1 did not alter the repetition/switching ratio (fig. S1M), whereas the inactivation of PrL significantly increased this ratio (fig. S1N), suggesting that PrL plays a key role in action switching.

To further elucidate the precise role of cortices in action sequence execution, we implanted optic fibers bilaterally into either the M1 or PrL of $Vgat^{Cre/+}$:Ai32 mice, through which the cortical projection neurons were temporarily inhibited by activating local GABAergic interneurons (*37*–*40*). In the trained $Vgat^{Cre/+}$:Ai32 mice, 1-s pulse of blue light (473 nm) was delivered at random half trials upon each lever press during LLRR sequence execution (Fig. 1F) to either M1 (Fig. 1, G to O; $n = 7$) or PrL (Fig. 1, P to X; $n = 6$). Intriguingly, the brief optogenetic silencing of M1 following the first L press suppressed the upcoming second L press and tended to reduce the total sequence length (Fig. 1, H and L; Wilcoxon matched-pairs signed rank test, length change under inhibition on the first left lever press, left: −0.36 ± 0.09, $P = 0.02$, right: 0.09 ± 0.08, $P = 0.3$, total: −0.27 ± 0.14, $P = 0.11$). Similar effects were observed on upcoming lever press and total sequence length for M1 silencing following the first R press (Fig. 1, J and N; Wilcoxon matched-pairs signed rank test, length change under inhibition on the first right lever press, left: 0.01 ± 0.09, $P = 0.30$, right: −0.27 ± 0.07, $P = 0.02$, total: −0.25 ± 0.12, $P = 0.03$). This suppression of ongoing lever pressing aligns with previous reports showing that photoinactivation of M1 transiently halts motor activity in animals (*40*). Temporal silencing of M1 following the second L or second R press had no effect either on upcoming lever press or on the total sequence length (Fig. 1, I and M; Wilcoxon matched-pairs signed rank test, length change under inhibition on the second left lever press, left: 0.05 ± 0.09, $P = 0.69$, right: −0.08 ± 0.09, $P = 0.69$, total: −0.04 ± 0.08, $P = 0.58$; Fig. 1, K and O; Wilcoxon matched-pairs signed rank test, length change under inhibition on the second right lever press, left: 0.04 ± 0.08, $P = 0.81$, right: 0.03 ± 0.03, $P = 0.38$, total: 0.11 ± 0.07, $P = 0.31$) due to the planned switching from L to R press and from the final R press to magazine entry, respectively. In contrast, the brief optogenetic silencing of PrL following each lever press during the LLRR sequence execution consistently induced the insertion of an additional ongoing lever press (Fig. 1, Q to X; Wilcoxon matched-pairs signed rank test, length change under inhibition on the first left lever press, left: 0.78 ± 0.16, $P = 0.03$, right: −0.62 ± 0.11, $P = 0.03$, total: 0.15 ± 0.12, $P = 0.31$; length change under inhibition on the second left lever press, left: 0.80 ± 0.15, $P = 0.03$, right: −0.38 ± 0.04, $P = 0.03$, total: 0.42 ± 0.16, $P = 0.07$; length change under inhibition on the first right lever press, left: −0.31 ± 0.14, $P = 0.06$, right: 0.72 ± 0.17, $P = 0.03$, total: 0.50 ± 0.22, $P = 0.09$; length change under inhibition on the second right lever press, left: 0.20 ± 0.07, $P = 0.06$, right: 1.16 ± 0.10, $P = 0.03$, total: 1.36 ± 0.13, $P = 0.03$). Notably, temporal silencing of PrL during the second L or second R press delayed the planned switches from L to R press and from the final R press to magazine entry (Fig. 1, R and V and T and X). The data indicate that optogenetic silencing of M1 reduces the action repetition within sequence, whereas optogenetic silencing of PrL delays action switching. Together, these results suggest that while both M1 and PrL are required for the performance of learned action sequence, they might be involved in controlling different aspects of action selection.

M1 and PrL encode distinct hierarchies of sequence structure

To further determine the potentially distinct functions of the M1 and PrL in action sequence execution, we implanted electrode

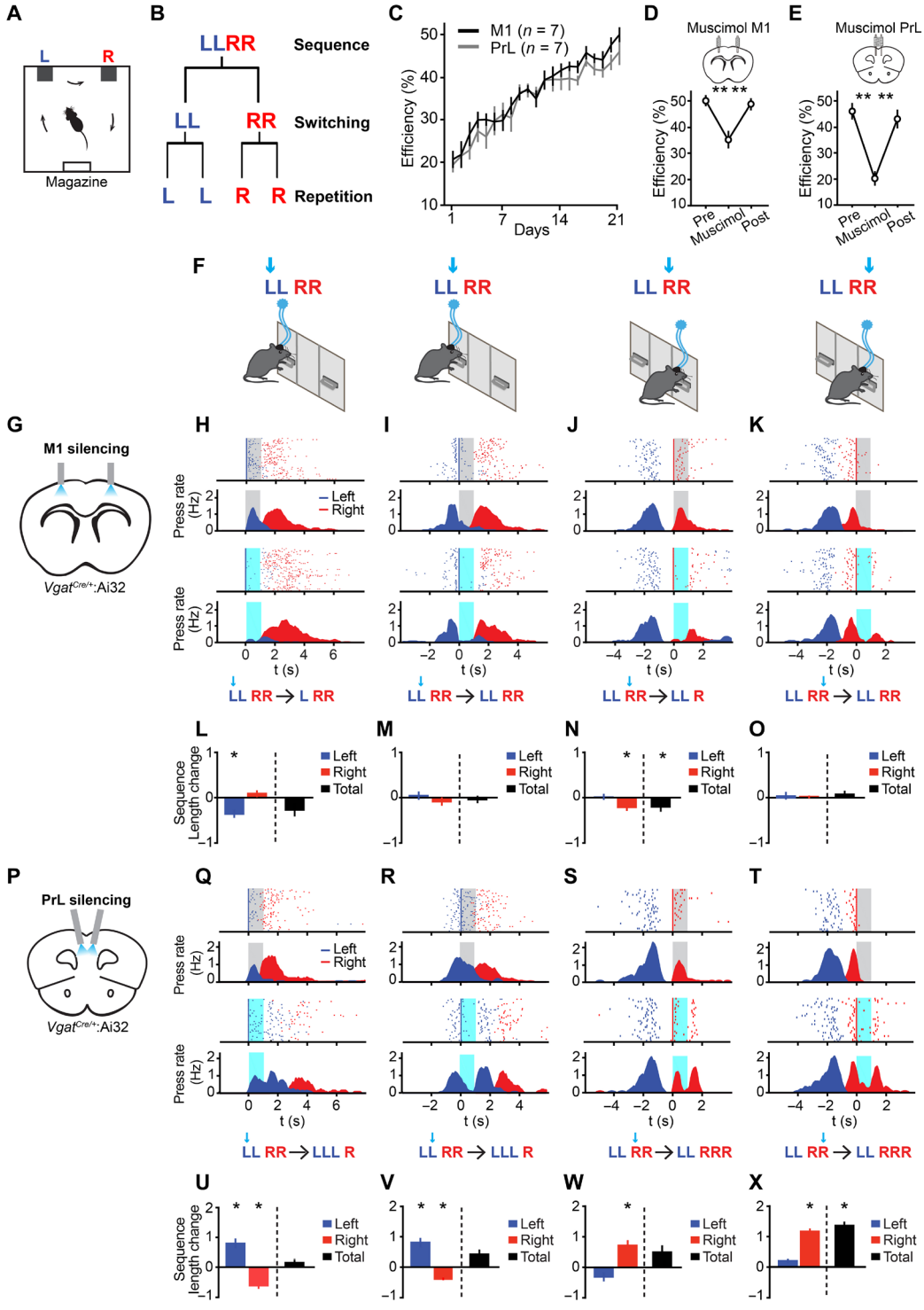

Fig. 1. Silencing M1 or PrL impaired learned sequence behavior. (**A**) Schematic of operant chamber used for the LLRR sequence behavior. (**B**) Action switching and action repetition in the LLRR sequence hierarchy. (**C**) Learning curve for the LLRR sequence behavior in the M1 and PrL group of mice. (**D** and **E**) Top: Diagram of cannula implantation for muscimol or saline infusion into M1 (D) and PrL (E). Bottom: Behavior efficiency under presaline, muscimol, and post-saline infusion into M1 (D) and PrL (E). (**F**) Protocol of optogenetic experiment. A 1-s light stimulation was triggered in random half of the trials by the first left, second left, first right, and second right lever press, respectively. (**G**) Diagram of M1 silencing. Optic fiber implanted into the M1 in *Vgat*$^{Cre/+}$:Ai32 mice. (**H** to **K**) Behavioral examples of M1 silencing following the first left (H), second left (I), first right (J), and second right (K) lever presses. Control conditions are shown with the supposed stimulation period covered in gray (top), while stimulated conditions are depicted with the stimulation period in light blue (bottom). Blue and red dashes and curves represent the left and right lever presses and press rates, respectively. Peri-event time histograms (PETHs) in all optogenetic experiments were plotted with excluding the referenced lever press in both control and stimulated conditions for illustration clarity. (**L** to **O**) Sequence length change after M1 silencing. The unit of length change is 1. (**P**) Diagram of PrL silencing. (**Q** to **T**) same as (H) to (K), but for PrL silencing. (**U** to **X**) Sequence length change after PrL silencing.

arrays into the M1 ($n = 5$ mice; Fig. 2B and fig. S2, A to C) or PrL ($n = 7$ mice; Fig. 2C and fig. S2, A, D, and E) to characterize sequence-related neuronal activities in trained mice performing the LLRR task (see Materials and Methods). It has been previously proposed that the learned LLRR action sequence can be organized into three hierarchical levels: sequence, subsequence, and element levels, respectively (*20*). Although many striatal neurons signal sequence-level start and stop, striatal D1-SPNs and D2-SPNs preferentially encode different hierarchical levels of sequence structure (*3*, *20*, *26*, *41*). More specifically, striatal D1-SPNs encode element level information and facilitate ongoing action when activated, while striatal D2-SPNs encode subsequence-level transition and trigger action switching when stimulated (*20*).

We recorded action-related, reward-related, and nonresponsive neurons in both M1 and PrL (fig. S2, F to H). Consistent with the previous analyses (*20*), we further categorized the action-related neuronal activity in M1 (174 neurons from five mice) and PrL (204 neurons from seven mice) into three hierarchical levels within the action sequence (see Materials and Methods). At the sequence level, we observed a significant proportion of neurons exhibiting sequence

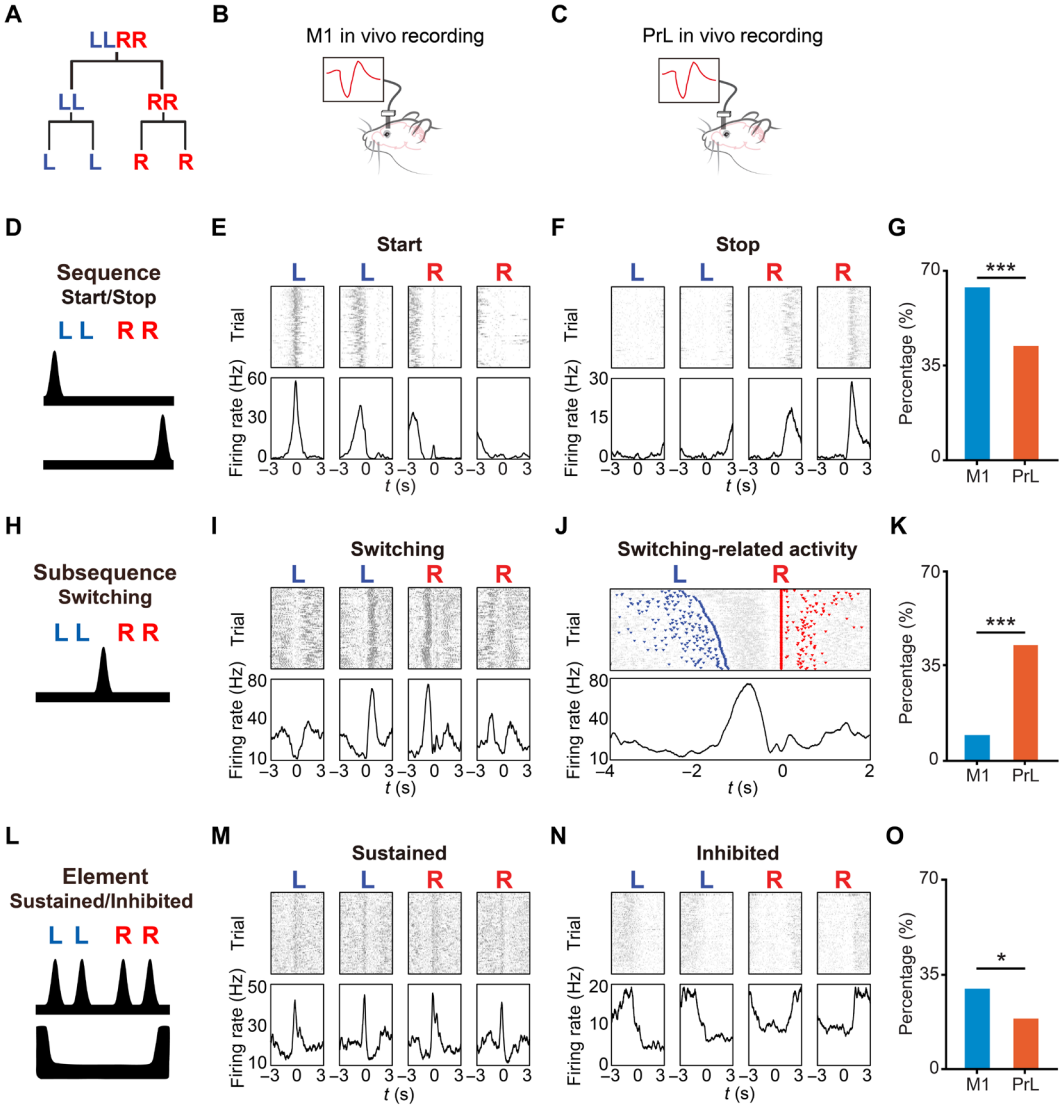

Fig. 2. M1 and PrL neurons encode different sequence hierarchies. (**A**) Action switching and action repetition in the LLRR sequence hierarchy. (**B**) Diagram showing M1 in vivo recording. (**C**) Diagram showing PrL in vivo recording. (**D**) Schematic of sequence start/stop neuronal activity at the sequence level. (**E**) Example of a neuron with start activity. Neuronal activity is aligned to the first left, second left, first right, and second right lever presses within the sequence, respectively. Top: Each black dash represents a spike. Bottom: PETH of neuronal firing rate. The same applies to (F), (I), (M), and (N). (**F**) Example of a neuron with stop activity. (**G**) Proportion of neurons in M1 and PrL neurons exhibiting start/stop activity. Two-proportion *z* test. (**H**) Schematic of subsequence switching neuronal activity. (**I**) Example of a neuron with switching activity. (**J**) Same neuron as shown in (I) with trials sorted by left-right subsequence switching intervals. Top: Left and right presses are marked by inverted blue and red triangles, respectively. Neuronal activity is aligned to the first right lever press. Bottom: PETH of neuronal firing rate. (**K**) Proportion of neurons in M1 and PrL exhibiting subsequence switching activity. Two-proportion *z* test. (**L**) Schematic of element sustained (top) and inhibited (bottom) neuronal activity at element level. (**M**) Example of a neuron with sustained activity. (**N**) Example of a neuron with inhibited activity. (**O**) Proportion of neurons in M1 and PrL showing element sustained/inhibited activity. Two-proportion *z* test.

start/stop-related activity in both M1 (n = 110, 63.2%) and PrL (n = 85, 41.7%) (z = −4.18, P < 0.00001; Fig. 2, D to G, and fig. S2I), indicating the potential contribution of cortices in organizing learned action sequences (*26*, *42*–*45*). Notably, the percentage of start but not stop neurons is significantly higher in M1 than PrL, suggesting a role of M1 in initiating action (fig. S2J). At the subsequence level, the "LL" to "RR" switch-related activity was found in both cortical regions (Fig. 2, H to J, and fig. S2I). Only 8.1% of M1 neurons (n = 14) exhibited switch-related activity, in contrast to 40.2% in PrL (n = 82), underscoring a possibly predominant role of PrL in action switching (z = −7.16, P < 0.00001; Fig. 2K and fig. S2J). At the element level, we identified the element-related sustained/inhibited activity, in which the neuron's firing was excited or suppressed throughout the whole LLRR sequence execution (Fig. 2, L to N, and fig. S2I). Notably, there was 28.7% of M1 neurons (n = 50) exhibited element-related activity compared to only 18.1% in PrL (n = 37), implying a specific role for M1 in controlling individual elemental actions, different from PrL (z = 2.44, P = 0.014; Fig. 2O and fig. S2J). These results reveal that although both M1 and PrL exhibit neuronal activities associated with all three levels of sequence hierarchies, M1 reflects more element-level information, whereas PrL encodes more subsequence-level switching (fig. S2J). Together with the optogenetic silencing results (Fig. 1), these data further suggest that M1 and PrL could mediate distinct hierarchies of sequence behavior. This functional distinction is likely mediated by the specific downstream structures targeted differently by M1 and PrL projections.

M1-DLS regulates action repetition, while PrL-DMS controls action switching

The dorsal striatum has been demonstrated as a critical center for action sequence execution (*20*), with M1 primarily innervating DLS (*46*) and PrL projecting to DMS (*35*, *36*). To causally test and differentiate the potentially distinct functions of M1 and PrL in sequence behavior, we next seek to optogenetically activate M1-DLS or PrL-DMS pathway in mice when they performed the learned LLRR sequence (Fig. 3A). To elucidate the function of M1 neurons that project to the dorsal striatum, we injected AAV2-retro-flp into the DLS and AAV5-fDIO-ChR2-YFP into the M1 and implanted optic fibers into M1 to selectively activate DLS-projecting M1 neurons (Fig. 3B and see Materials and Methods). Notably, the optogenetic activation of the DLS-projecting M1 neurons following each lever press within the LLRR sequence consistently promoted animals to press additional ongoing press (Fig. 3, C to F; n = 7), regardless of whether it is first L, second L, first R, or second R press (Fig. 3, G to J; length change under stimulation on the first left lever press, left: 0.58 ± 0.10, P = 0.02; right: −0.33 ± 0.10, P = 0.03; total: 0.25 ± 0.08, P = 0.02; length change under stimulation on the second left lever press, left: 0.45 ± 0.09, P = 0.02; right: −0.23 ± 0.10, P = 0.08; total: 0.21 ± 0.13, P = 0.22; length change under stimulation on the first right lever press, left: −0.05 ± 0.06, P = 0.81; right: 0.44 ± 0.06, P = 0.02; total: 0.39 ± 0.10, P = 0.02; length change under stimulation on the second right lever press, left: −0.005 ± 0.05, P = 0.69; right: 0.36 ± 0.04, P = 0.03; total: 0.36 ± 0.08, P = 0.30). These effects were further confirmed with optogenetic activation using various durations or frequencies (fig. S3, A to F), indicating a causal role of M1-DLS pathway in facilitating action repetition. To verify the optogenetic effects of M1 were mediated through the striatum, we injected AAV9-hsyn-ChR2-eYFP (enhanced yellow fluorescent protein) into M1 and correspondingly implanted optic fibers to activate its terminals in DLS following each lever press (Fig. 4, B to J; n = 7, length change under stimulation on the first left lever press, left: 0.35 ± 0.05, P = 0.02; right: −0.18 ± 0.08, P = 0.11; total: 0.17 ± 0.12, P = 0.30; length change under stimulation on the second left lever press, left: 0.27 ± 0.09, P = 0.02; right: −0.16 ± 0.06, P = 0.06; total: 0.10 ± 0.12, P = 0.58; length change under stimulation on the first right lever press, left: −0.26 ± 0.05, P = 0.05; right: 0.32 ± 0.05, P = 0.02; total: 0.06 ± 0.08, P = 0.47; length change under stimulation on the second right lever press, left: −0.03 ± 0.04, P = 0.69; right: 0.17 ± 0.07, P = 0.08; total: 0.13 ± 0.07, P = 0.08). Similarly, the optogenetic activation of M1 terminals in DLS recapitulated the effects of stimulating DLS-projecting M1 neuronal soma by increasing action repetition (Fig. 4, B to J). Consistent with the in vivo neuronal recording data, these results suggest that M1 neurons control elemental execution within sequence, and activation of M1-DLS pathway facilitates action repetition.

Next, we injected AAV2-retro-flp into the DMS and AAV5-fDIO-ChR2-YFP into the PrL to selectively activate DMS-projecting PrL neurons during sequence execution (Fig. 3, K to S; n = 7). Strikingly, optogenetic activation of the DMS-projecting PrL neurons upon the first L press eliminated the following left lever presses, inducing a direct switch to the right subsequence and shorter total sequence length (Fig. 3, L and P; length change under stimulation on the first left lever press, left: −0.86 ± 0.14, P = 0.02; right: 0.26 ± 0.16, P = 0.16; total: −0.60 ± 0.18, P = 0.02). Similarly, the activation of the DMS-projecting PrL neurons upon the first R press reduced the following right lever presses and decreased the total sequence length (Fig. 3, N and R; length change under stimulation on the first right lever press, left: −0.009 ± 0.09, P = 0.94; right: −0.76 ± 0.16, P = 0.02; total: −0.77 ± 0.18, P = 0.02). Optogenetic stimulation of PrL on the second L or second R press caused no changes on the sequence structure due to the planned switching following these actions (Fig. 3, M and Q; length change under stimulation on the second left lever press, left: −0.04 ± 0.09, P = 0.30; right: −0.10 ± 0.14, P = 0.58; total: −0.15 ± 0.14, P = 0.30, O and S, length change under stimulation on the second right lever press, left: −0.05 ± 0.21, P = 0.81; right: −0.17 ± 0.13, P = 0.30; total: −0.41 ± 0.22, P = 0.16). Again, these behavioral effects were replicated with optogenetic activation with various duration or frequency (fig. S3, G to L), underscoring a causal role for DMS-projecting PrL neurons in action switching. Furthermore, the optogenetic stimulation of PrL neuronal terminals in DMS (Fig. 4, K to S; n = 8, length change under stimulation on the first left lever press, left: −0.43 ± 0.08, P = 0.009; right: 0.10 ± 0.12, P = 0.46; total: −0.34 ± 0.10, P = 0.02; length change under stimulation on the second left lever press, left: −0.01 ± 0.16, P = 0.95; right: 0.24 ± 0.14, P = 0.20; total: −0.25 ± 0.18, P = 0.25; length change under stimulation on the first right lever press, left: −0.05 ± 0.13, P = 0.84; right: −0.60 ± 0.09, P = 0.009; total: −0.65 ± 0.10, P = 0.009; length change under stimulation on the second right lever press, left: 0.03 ± 0.10, P = 0.64; right: 0.04 ± 0.09, P = 0.74; total: 0.07 ± 0.16, P = 0.64), but not collaterals in other downstream regions including the claustrum, mediodorsal thalamus, or amygdala (fig. S4), recapitulated the effects of PrL soma activation. Consistent with the finding of substantial switch-related neuronal activity in PrL, these data demonstrate that activation of PrL-DMS pathway triggers action switching. Collectively, these results suggest that the M1-DLS circuit regulates action repetition, while the PrL-DMS pathway controls action switching.

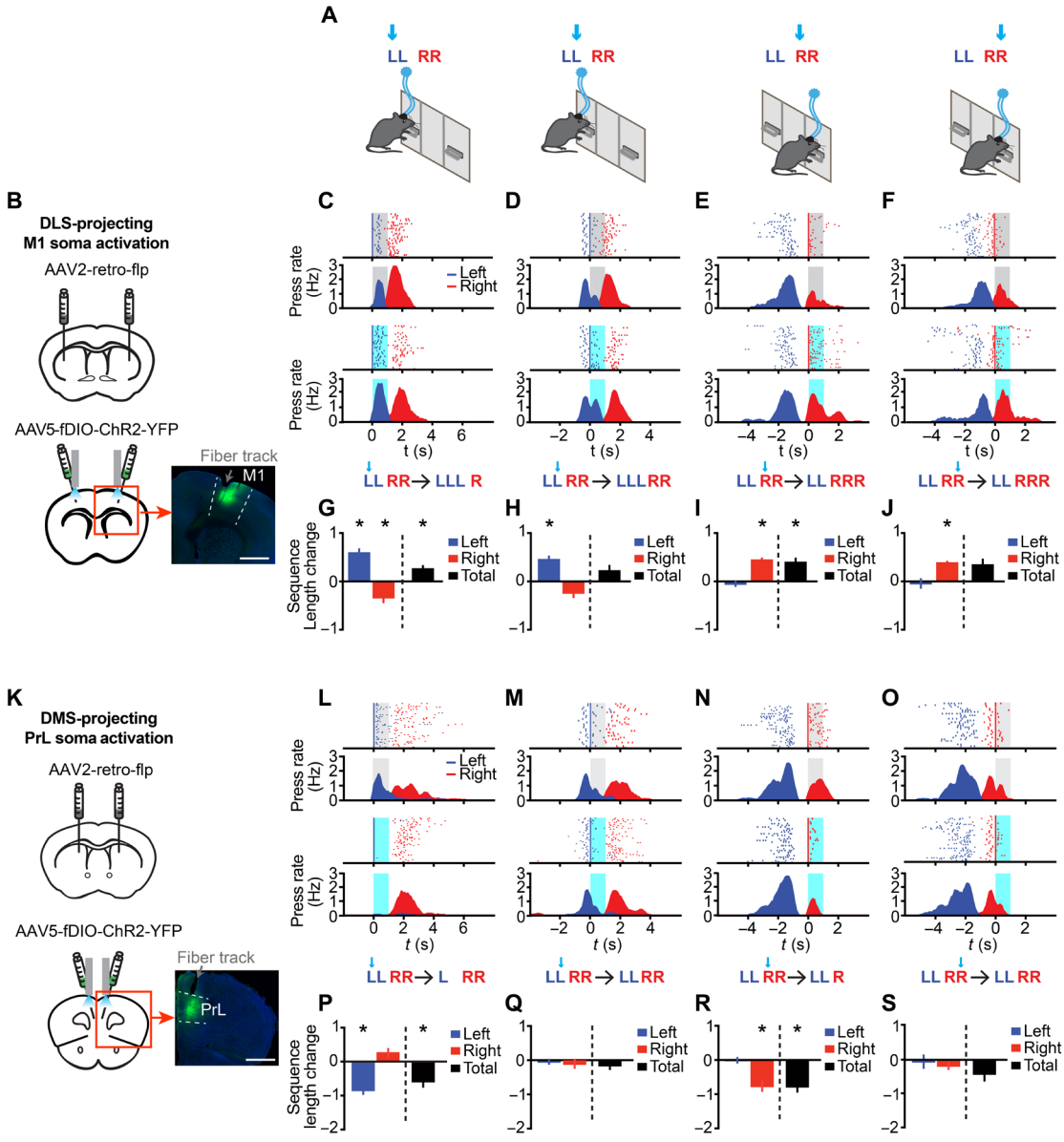

Fig. 3. Optogenetic stimulation of DLS-projecting M1 neurons facilitates action repetition, while activation of DMS-projecting PrL neurons triggers action switching. (**A**) Protocol for optogenetic experiment. Light stimulation (1 s) was triggered in random half of the trials by the first left, second left, first right, or second right lever press within the sequence, respectively. (**B**) Diagram of opto-activation of DLS-projecting M1 neurons in WT mice. AAV2-retro-flp was injected into the DLS, AAV5-fDIO-ChR2-YFP was injected into M1 area, and optic fiber was implanted to M1. Bottom right: Example slice showing virus expression and fiber track in M1. Scale bar, 1 mm. (**C** to **F**) Behavioral examples of DLS-projecting M1 activation following the first left (C), second left (D), first right (E), and second right (F) lever presses. (**G** to **J**) Sequence length changes after DLS-projection M1 activation. All tests went through the Wilcoxon matched-pairs signed rank test. (**K**) Diagram of opto-activation of DMS-projecting PrL neurons in WT mice. AAV2-retro-flp was injected into DMS, AAV5-fDIO-ChR2-YFP was injected into PrL, and optic fiber was implanted to PrL. Bottom right: Example slice showing virus expression and fiber track in PrL. Scale bar, 1 mm. (**L** to **O**) Same as (C) to (F), but for DMS-projecting PrL activation following the first left (L), second left (M), first right (N), and second right (O) lever presses in the sequence. (**P** to **S**) Sequence length changes after DMS-projection PrL activation. All tests went through the Wilcoxon matched-pairs signed rank test.

Biased innervation from M1 to D1-SPNs and PrL to D2-SPNs

It has been previously demonstrated that the striatal direct pathway D1-SPNs are instrumental in facilitating ongoing actions (*20*), consistent with the result of M1 optogenetics. In contrast, the striatal indirect pathway D2-SPNs mediate subsequence switching (*20*), in line with the PrL optogenetics effects. During the LLRR sequence execution, the sequence-related activity in M1 and PrL (Fig. 2) closely resemble the functional profile of striatal D1- and D2-SPNs, respectively (*20*). We thus decided to dissect the pathway-specific corticostriatal subcircuits and asked whether there are any preferential innervations from these two cortical regions to striatal D1- versus D2-SPNs. Here, AAV9-hsyn-ChR2-eYFP was injected into the

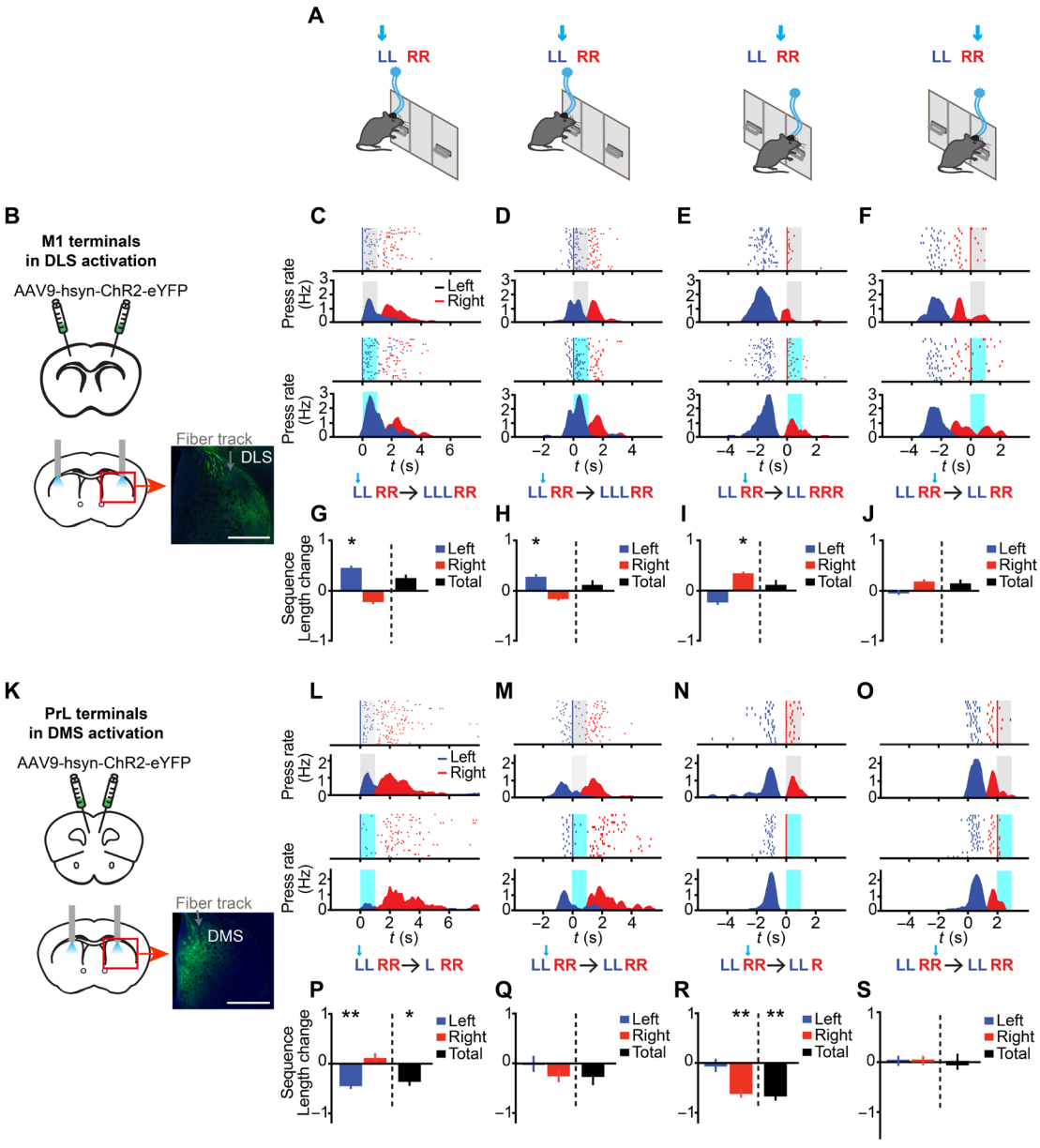

Fig. 4. Activation of M1 or PrL neuronal terminals in the striatum facilitates action repetition or induces action switching, respectively. (**A**) Protocol for optogenetic experiment. (**B**) Diagram showing opto-stimulation of M1 terminals in DLS of WT mice. AAV9-hsyn-ChR2-eYFP was injected into M1, and optic fiber was implanted in the DLS. Bottom right: Example slice showing virus expression and fiber track in DLS. Scale bar, 1 mm. (**C** to **F**) Behavioral examples of M1 terminals stimulation in DLS following the first left (C), second left (D), first right (E), and second right (F) lever presses under control conditions (top two panels) and stimulated conditions (bottom two panels). (**G** to **J**) Sequence length changes after stimulation of M1 terminals in DLS. All tests went through the Wilcoxon matched-pairs signed rank test. (**K**) Diagram of opto-stimulation of PrL terminals in DMS of WT mice. AAV9-hsyn-ChR2-eYFP was injected into PrL, and optic fiber was implanted into DMS. Bottom right: Example slice showing virus expression and fiber track in DMS. Scale bar, 1 mm. (**L** to **O**) Same as (C) to (F), but for stimulation of PrL terminals in DMS following the first left (L), second left (M), first right (N), and second right (O) lever presses. (**P** to **S**) Sequence length changes after stimulation of PrL terminals in DMS. All tests went through the Wilcoxon matched-pairs signed rank test.

M1 or PrL, and single-cell patch recordings were then performed in brain slices, with optogenetic stimulation of cortical terminals in the corresponding striatal subregions (Fig. 5, A and D). D2- and D1-SPNs were identified by using either D2–enhanced green fluorescent protein (EGFP) mice or D1-Cre mice with AAV5-flex-mCherry injected (Fig. 4, B and E, and see Materials and Methods). It was found that optogenetic activation of M1 terminals in DLS evoked excitatory postsynaptic currents (EPSCs) in striatal SPNs, which were completely blocked by bath application of 2,3-dihydroxy-6-nitro-7-sulfamoylbenzo[f]quinoxaline (NBQX, an AMPA receptor antagonist) and DL-2-amino-5-phosphonovalericacid (DL-APV, an NMDA receptor antagonist) (Fig. 5B). Notably, EPSCs recorded from D1-SPNs were significantly larger than those recorded from D2-SPNs (Fig. 5, B and C; EPSCs of D1-SPNs: 230.30 ± 33.12 pA,

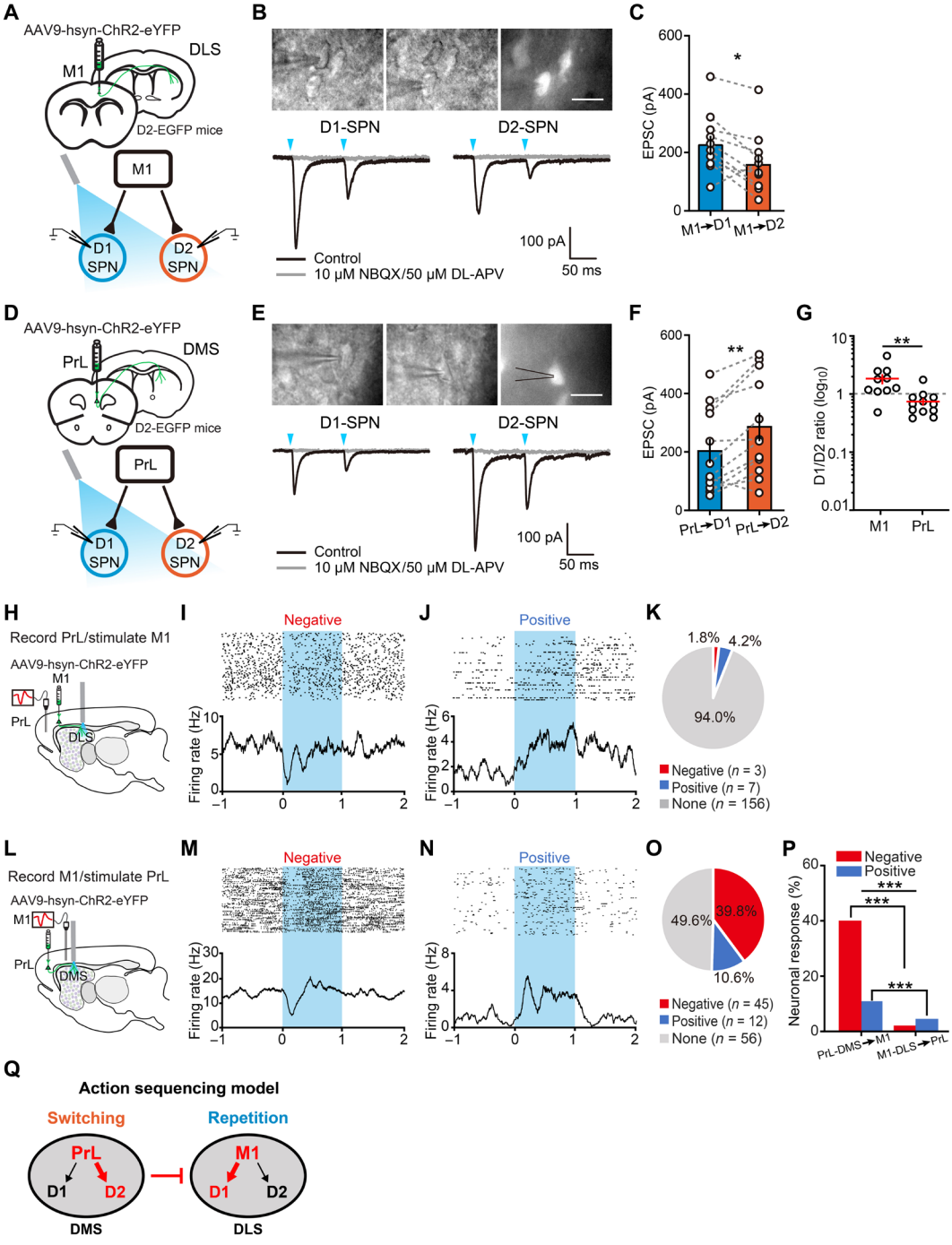

Fig. 5. Preferential innervations from M1 to striatal D1-SPNs and from PrL to striatal D2-SPNs, respectively. (**A**) Diagram of slice recordings of D1- and D2-SPNs in the DLS during activation of M1 terminals. (**B**) Example of evoked EPSCs in D1- and D2-SPNs during activation of M1 terminals. Top: D1-SPNs without fluorescence and D2-SPNs with fluorescence. Scale bar, 10 μm. Bottom: optogenetic evoked EPSCs in D1- and D2-SPNs. (**C**) Statistics of evoked EPSCs in D1- and D2-SPNs during activation of M1 terminals. (**D**) Diagram of slice recordings of D1- and D2-SPNs in the DMS when activating PrL terminals. (**E**) Example of evoked EPSCs in D1- and D2-SPNs during activation of PrL terminals. (**F**) Statistics of evoked EPSCs in D1- and D2-SPNs during activation of PrL terminals. (**G**) The ratio of evoked EPSCs in D1- and D2-SPNs for M1 and PrL terminals activation. (**H**) Diagram of in vivo acute recording of PrL neurons when stimulating M1 terminals in the DLS. (**I** and **J**) Example of negative (I) and positive (J) responsive neurons in the PrL. Blue shadow indicates 1-s optogenetic stimulation. (**K**) Pie chart indicating the proportion of negative (red), positive responsive (blue), and nonresponsive PrL neurons (gray) when stimulating M1 terminals in DLS. (**L**) Diagram of in vivo acute recording of M1 neurons when stimulating PrL terminals in DMS. (**M** and **N**) Example of negative (M) and positive (N) responsive neurons in M1. (**O**) Same as (K), but for M1 with stimulating PrL terminals in DMS. (**P**) Comparison of the percentage of M1 or PrL responsive neurons under optogenetic stimulation of PrL-DMS pathway or M1-DLS pathway, respectively. (**Q**) Diagram of action sequencing model. Action repetition is regulated by the M1-DLS pathway through D1-SPNs. Action switching is controlled by the PrL-DMS pathway through D2-SPNs. When activated, the switching mode overwrites the repetition mode through the unidirectional inhibition from PrL-DMS pathway to M1.

EPSCs of D2-SPNs: 162.50 ± 33.83 pA, $n = 10$ pairs, paired t test, $P = 0.01$), suggesting that M1 has stronger excitatory innervations on striatal D1-SPNs than the D2-SPNs. On the contrary, optogenetic activation of PrL terminals in DMS elicited larger EPSCs in D2-SPNs than D1-SPNs (Fig. 5, D to F; D1-SPNs: 207.7 ± 41.43 pA, D2-SPNs: 290.70 ± 48.74 pA, $n = 12$ pairs, paired t test, $P = 0.001$), indicating the preferential innervations from PrL neurons to the D2-SPNs. The significant difference in the D1/D2-SPNs EPSCs ratios between M1 and PrL terminal activation highlights their biased projections to D1-SPNs and D2-SPNs, respectively (Fig. 5G; D1/D2 ratio of M1 terminal stimulation: 1.84 ± 0.36, $n = 10$; D1/D2 ratio of PrL terminal stimulation: 0.74 ± 0.11, $n = 12$; unpaired t test, $P = 0.005$).

It has been recently reported that there exists an anatomical pathway allowing limbic control over motor output through the nigrothalamic circuit among the cortico-basal ganglia loops (*36*). During action sequence execution, the brain must coordinate action repetition and switching to enable appropriate momentary action selection (*2*–*4*). To investigate how these two neural machineries interact in vivo, we aim to evaluate the modulation effects on M1-DLS circuit by optogenetic activation of PrL-DMS pathway and vice versa. AAV9-hsyn-ChR2-eYFP was injected into M1 of wild-type (WT) mice, and in vivo neuronal recordings in the PrL were later performed with optogenetic stimulation of M1 terminals in DLS (Fig. 5H and see Materials and Methods). Among all PrL neurons recorded ($n = 166$), 1.8% exhibited inhibitory responses (Fig. 5I; latency: 44.7 ± 8.3 ms), and 4.2% showed excitatory responses (Fig. 5J; latency: 340.1 ± 76.9 ms) while the majority showing no significant modulation on the firing rate (Fig. 5K) to M1 stimulation. When the similar experiments were performed with PrL-DMS stimulation and M1 recording (Fig. 4L; $n = 113$ neurons), it was found inhibitory response in 39.8% (Fig. 5M; latency: 58.6 ± 5.3 ms) and excitatory response in 10.6% of M1 neurons (Fig. 5N; latency: 131.6 ± 12.7 ms), respectively (Fig. 5O). These results suggest while stimulating the M1-DLS pathway has negligible effects on PrL, the activation of the PrL-DMS pathway strongly inhibits M1 activity (Fig. 5P; two-proportion z test, total neural response between M1 and PrL: $P < 0.0001$; negative response between PrL-DMS to M1 and M1-DLS to PrL: $P < 0.0001$; positive response between PrL-DMS to M1 and M1-DLS to PrL: $P < 0.0001$), implying a unidirectional inhibition from the action switching to action repetition circuit (Fig. 5Q).

To further elucidate the competition between the M1-DLS action repetition and PrL-DMS action switching pathway at the behavior level, we seek to activate both pathways simultaneously during sequence performance. AAV2-retro-flp was bilaterally injected into both DLS and DMS of WT mice, followed by bilateral AAV5-fDIO-ChR2-YFP injection into both M1 and PrL with optic fibers implanted for optogenetically stimulating these two cortical regions (Fig. 6, B and K, and see Materials and Methods). The behavioral effects of activating M1 individually on facilitating action repetition during sequence behavior were first verified in these mice (Fig. 6, C to J; $n = 6$, length change under stimulation on the first left lever press, left: 0.69 ± 0.22, $P = 0.03$; right: −0.24 ± 0.31, $P = 0.93$; total: 0.45 ± 0.12, $P = 0.03$; length change under stimulation on the second left lever press, left: 0.54 ± 0.15, $P = 0.03$; right: −0.29 ± 0.14, $P = 0.18$; total: 0.25 ± 0.13, $P = 0.16$; length change under stimulation on the first right lever press, left: −0.25 ± 0.21, $P = 0.82$; right: 0.59 ± 0.17, $P = 0.03$; total: 0.29 ± 0.18, $P = 0.09$; length change under stimulation on the second right lever press, left: −0.08 ± 0.08, $P = 0.71$; right: 0.44 ± 0.08, $P = 0.03$; total: 0.37 ± 0.15, $P = 0.06$). Notably, simultaneous activation of M1 and PrL following each lever press reduced action repetition and promoted action switching (Fig. 6, L to S; $n = 6$, length change under stimulation on the first left lever press, left: −0.57 ± 0.07, $P = 0.03$; right: 0.06 ± 0.12, $P = 0.69$; total: −0.51 ± 0.11, $P = 0.03$; length change under stimulation on the second left lever press, left: −0.21 ± 0.08, $P = 0.06$; right: 0.18 ± 0.18, $P = 0.34$; total: −0.04 ± 0.17, $P = 0.73$; length change under stimulation on the first right lever press, left: 0.03 ± 0.15, $P = 0.39$; right: −0.44 ± 0.05, $P = 0.03$; total: −0.41 ± 0.14, $P = 0.06$; length change under stimulation on the second right lever press, left: 0.14 ± 0.21, $P = 0.56$; right: −0.24 ± 0.13, $P = 0.09$; total: −0.10 ± 0.17, $P = 0.63$), an effect similar with activation of PrL-DMS pathway alone (Fig. 3). These observations are in consistent with the electrophysiological data showing unidirectional inhibition from the PrL-DMS pathway to M1, ensuring a dominant behavioral effect of action switching on action repetition (Fig. 5Q). Together, these results suggest that the M1-DLS pathway mediates action repetition, while the PrL-DMS pathway controls action switching. These functions are implemented through biased projections from M1 to striatal D1-SPNs and PrL to D2-SPNs, respectively. The action switching behavioral mode exerts a dominant effect and is capable to override the action repetition mode via unidirectional inhibition from the PrL-DMS pathway to M1 through cortico-basal ganglia loops.

Deficient sequence behavior in *Shank3* KO mice

Because distinct corticostriatal circuits mediate action repetition and switching, which are crucial for action sequencing, we thus asked what goes awry in the neural circuits of neurological and psychiatric disorders that impair sequence behavior. One such condition is ASD, which is characterized by repetitive and stereotyped behaviors (*16*, *17*). Based on our switching-repetition model (fig. S5A), the excessive stereotyped behaviors observed in these conditions could result from either enhanced M1-DLS pathway–mediated action repetition (fig. S5B) or weakened PrL-DMS pathway–controlled action switching (fig. S5C). To investigate these mechanisms in the context of ASD, we used mouse mutants with *Shank3* gene deletion, known to exhibit not only social deficits but also repetitive behaviors such as excessive grooming (*33*). Specifically, in the *Shank3* $^{fx/fx}$ (referred to *Shank3* KO) mice, the *Shank3* gene was initially knocked out but can be restored following *Cre* expression (*47*). When *Shank3* KO mice and their littermate controls were trained under the LLRR action sequence task, the *Shank3* KOs showed minimal improvement over 21 days and exhibited significant impairments in sequence learning compared to the littermate controls (Fig. 7, A and B; effect across training: $F_{2,22} = 17.91$, $P < 0.0001$; Tukey's multiple comparison test, littermate ctrl versus *Shank3* KO, $P < 0.0001$; *Shank3* het versus *Shank3* KO, $P < 0.0001$; littermate ctrl versus *Shank3* het, $P = 0.80$).

Further analysis revealed that not only was the ratio of repetition versus switching significantly higher in *Shank3* KO group (Fig. 7C; littermate ctrl: 1.91 ± 0.11, $n = 8$, black bar; *Shank3* het: 1.87 ± 0.09, $n = 9$, gray bar; *Shank3* KO: 3.78 ± 0.46, $n = 8$, red bar. One-way analysis of variance (ANOVA) with Tukey's multiple comparison test: littermate ctrl versus *Shank3* het: $P > 0.99$; littermate ctrl versus *Shank3* KO: $P = 0.0019$; *Shank3* het versus *Shank3* KO: $P = 0.0009$; fig. S6), but the repetitive grooming in home cage was also increased in these mice (fig. S7B, red bar), indicating that *Shank3* KO mice are severely compromised in both innate and learned sequence behavior

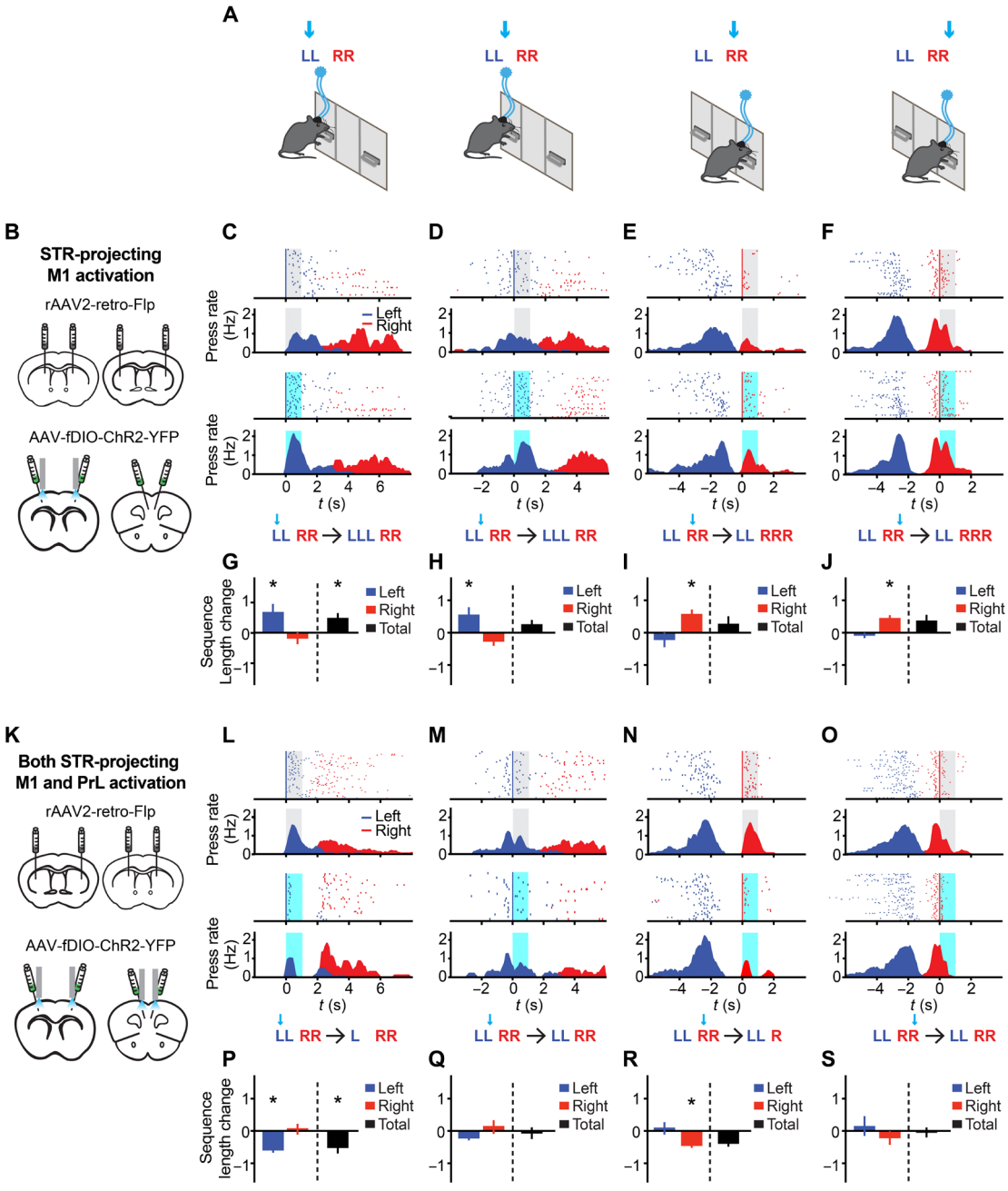

Fig. 6. Simultaneous activation of both the M1-DLS and PrL-DMS pathways triggers action switching. (**A**) Protocol for optogenetic experiment. (**B**) Diagram showing opto-stimulation of striatal projecting M1 neurons in WT mice. AAV2-retro-flp was injected into both the DLS and DMS, and AAV5-fDIO-ChR2-YFP was injected into the M1 and PrL. For activation of striatal-projecting M1, blue light was shined only through the optic fiber in M1. (**C** to **F**) Behavioral examples of striatal projecting M1 neurons stimulation following the first left (C), second left (D), first right (E), and second right (F) lever presses under control conditions (top) and stimulated conditions (bottom). (**G** to **J**) Sequence length changes after striatal-projecting M1 neurons activation in WT mice. All tests went through the Wilcoxon matched-pairs signed rank test. (**K**) Same group of mice in (B), but for activation of both striatal-projecting M1 and PrL, blue light was shined simultaneously in both M1 and PrL. (**L** to **O**) Behavioral examples of both striatal-projecting PrL and M1 neurons stimulation following the first left (L), second left (M), first right (N), and second right (O) lever presses of the sequence. Same as (C) to (F). (**P** to **S**) Sequence length changes after simultaneous stimulation of striatal-projecting PrL and M1 neurons. All tests went through the Wilcoxon matched-pairs signed rank test.

due to excessive action repetition (*48*). We thus seek to probe the specific functions of M1-DLS and PrL-DMS pathways in *Shank3* KO mice during the execution of LLRR action sequences. Similar with the procedures in WT mice, AAV2-retro-flp was injected into the DLS or DMS with AAV5-fDIO-ChR2-YFP into the M1 or PrL correspondingly in *Shank3* KO mice, followed by optogenetic stimulation of striatum-projecting M1 (Fig. 7, D to M) or PrL neurons during sequence execution (Fig. 7, N to V and see Materials and Methods). Unlike WT mice, the activation of DLS-projecting M1 neurons had no detectable effects on sequence behavior in the *Shank3* KO mice, whether the stimulation is on first, second, third, or fourth lever press (Fig. 7, F to M; $n = 6$, length change under

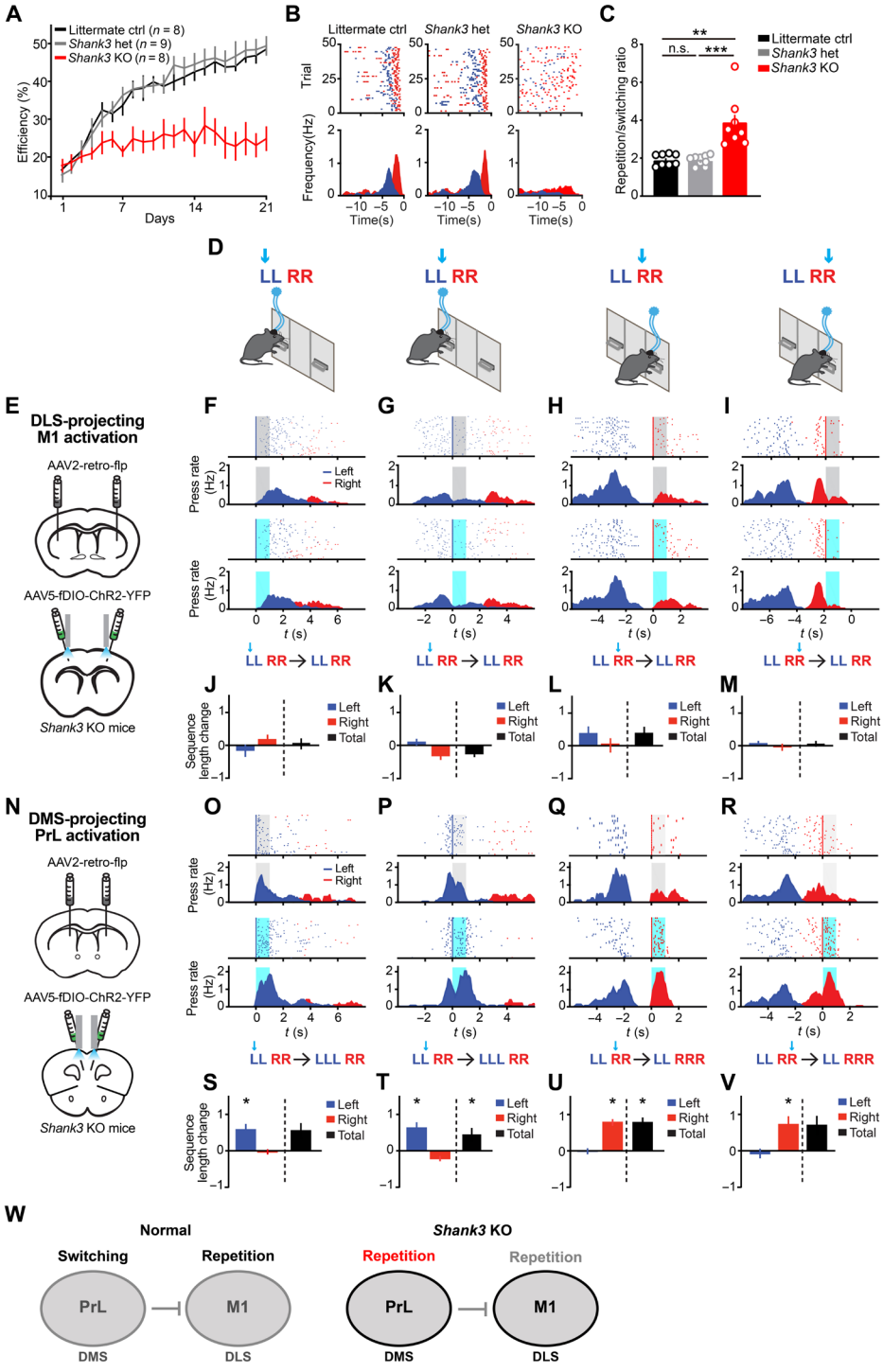

Fig. 7. Impaired sequence learning and deficient action switching in *Shank3* KO mice. (**A**) Learning curve of the LLRR sequence behavior in littermate control *Shank3*$^{+/+}$ mice (littermate ctrl, black), *Shank3*$^{fx/+}$ mice (*Shank3* het, gray), and *Shank3*$^{fx/fx}$ mice (*Shank3* KO, red). (**B**) Examples of mouse behavior on the last day of training. Left: Littermate ctrl; middle: *Shank3* het; right: *Shank3* KO. Sequences were aligned to magazine entry as time zero. (**C**) Repetition versus switching ratio was defined as the percentage of repetition lever presses (LL or RR) divided by switching lever presses (LR or RL) within a session on the last day of training. (**D**) Protocol of optogenetic experiment. (**E**) Diagram of opto-activation of DLS-projecting M1 neurons in *Shank3* KO mice. (**F** to **I**) Behavioral examples of DLS-projecting M1 neurons stimulation in *Shank3* KO mice. (**J** to **M**) Sequence length change after DLS-projecting M1 neurons activation in *Shank3* KO mice. All tests went through the Wilcoxon matched-pairs signed rank test. (**N**) Diagram of opto-activation of DMS-projecting PrL neurons in *Shank3* KO mice. (**O** to **R**) Behavioral examples of DMS-projecting PrL neurons stimulation in *Shank3* KO mice. (**S** to **V**) Sequence length change after DMS-projecting PrL neurons activation in *Shank3* KO mice. All tests went through the Wilcoxon matched-pairs signed rank test. (**W**) Diagram of action sequencing model in WT mice (left) and *Shank3* KO mice (right). Right: In *Shank3* KO mice, function of the PrL-DMS pathway, instead of controlling action switching, turns into regulating action repetition.

stimulation on the first left lever press, left: −0.16 ± 0.06, $P = 0.35$; right: 0.20 ± 0.04, $P = 0.18$; total: 0.07 ± 0.05, $P = 0.64$; length change under stimulation on the second left lever press, left: 0.10 ± 0.04, $P = 0.37$; right: −0.35 ± 0.04, $P = 0.06$; total: −0.25 ± 0.03, $P > 0.05$; length change under stimulation on the first right lever press, left: 0.39 ± 0.07, $P = 0.12$; right: 0.01 ± 0.08, $P = 0.97$; total: 0.40 ± 0.06, $P = 0.06$; length change under stimulation on the second right lever press, left: 0.07 ± 0.02, $P = 0.27$; right: −0.01 ± 0.03, $P = 0.88$; total: 0.06 ± 0.02, $P = 0.40$). Meanwhile, the activation of the DMS-projecting PrL neurons in the *Shank3* KO mice, instead of triggering action switching same as observed in WT mice, facilitated action repetition at each press within sequence (Fig. 7, O to V; $n = 7$, length change under stimulation on the first left lever press, left: 0.58 ± 0.16, $P = 0.02$; right: −0.03 ± 0.07, $P = 0.78$; total: 0.55 ± 0.22, $P = 0.08$; length change under stimulation on the second left lever press, left: 0.63 ± 0.16, $P = 0.03$; right: −0.21 ± 0.07, $P = 0.06$; total: 0.45 ± 0.18, $P = 0.03$; length change under stimulation on the first right lever press, left: −0.004 ± 0.08, $P = 0.94$; right: 0.78 ± 0.09, $P = 0.02$; total: 0.77 ± 0.14, $P = 0.02$; length change under stimulation on the second right lever press, left: −0.073 ± 0.13, $P = 0.69$; right: 0.72 ± 0.23, $P = 0.04$; total: 0.69 ± 0.26, $P = 0.08$). These results suggest that the repetitive behaviors observed in *Shank3* KO mice are not due to enhanced action repetition function in the M1-DLS pathway but are likely a consequence of an altered PrL-DMS circuit in which it now facilitates action repetition (Fig. 7W).

Altered pathway-specific corticostriatal projections in *Shank3* KO mutants

To elucidate the circuit mechanisms underlying the deficient sequence behavior observed in *Shank3* KO mice, we performed slice recordings to evaluate the corticostriatal synapses from M1 and PrL to striatal D1- and D2-SPNs in these mutants. AAV9-hsyn-ChR2-eYFP was injected into the M1 or PrL of D2-EGFP:*Shank3* KO mice followed by optogenetic activation of corresponding cortical terminals in the striatum (Fig. 8, A and B). Notably, when optogenetic stimulation of M1 terminals was applied, there tends to be a greater amplitude of EPSCs recorded in D1-SPNs compared to D2-SPNs (Fig. 8B, left; EPSCs of D1-SPNs: 54.0 ± 9.1 pA, D2-SPNs: 43.0 ± 9.7 pA, $n = 8$ pairs; paired *t* test: M1 to D1-SPNs versus M1 to D2-SPNs, $P = 0.13$), and the D1/D2 ratio from M1 to DLS is comparable to that in WT mice (Fig. 8C, left; 1.5 ± 0.32, $n = 8$ pairs, and Fig. 5G, unpaired *t* test, D1/D2 ratio from M1 to DLS between WT and *Shank3* KO mice: $P = 0.49$). Surprisingly, activation of PrL terminals resulted in significantly larger EPSCs in D1-SPNs compared to D2-SPNs in DMS (Fig. 8B, right; EPSCs of D1-SPNs: 55.8 ± 11.0 pA, D2-SPNs: 37.0 ± 8.3 pA, $n = 10$ pairs; paired *t* test: PrL to D1-SPNs versus PrL to D2-SPNs, $P = 0.03$). Consequently, the D1/D2 ratio from PrL to DMS significantly exceeded one in *Shank3* KO mice (Fig. 8C, right; 1.69 ± 0.19, $n = 10$ pairs, comparison of D1/D2 ratio between M1 and PrL groups went through unpaired *t* test, $P = 0.58$.), a reversal from WT mice (Fig. 5G; unpaired *t* test, the D1/D2 ratio from PrL to DMS between WT and *Shank3* KO mice: $P = 0.0002$). Together, these data unveiled comparable innervations from M1 to striatal D1-SPNs versus D2-SPNs in *Shank3* KO animals but a reversal of the D1/D2 ratio in the PrL-DMS pathway in which PrL drives largely striatal D1-SPNs.

Given the reversed D1/D2 ratio in the PrL-DMS pathway of *Shank3* KO mice, we wondered whether the unidirectional inhibition from PrL-DMS circuit to M1 found in WT mice was also altered in these mutants. To examine this, we performed in vivo extracellular recordings from M1 neurons ($n = 121$) of *Shank3* KO mice while optogenetically activating PrL terminals in DMS (Fig. 8D). Among the M1 cells that responded, very few showed inhibitory response during activation of PrL terminals (Fig. 8, E and G; latency: 58.7 ± 27.2 ms), while the majority exhibited excitatory response (Fig. 8, F and G; latency: 203.6 ± 12.6 ms), qualitatively opposite to the responses seen in WT mice (Fig. 5O; two-proportion *z* test, negative response between WT and *Shank3* KO mice: $z = -6.4552$, $P < 0.00001$, positive response between WT and *Shank3* KO mice: $z = 1.6404$, $P = 0.101$). Therefore, the predominant effect of PrL-DMS pathway activation on M1 shifts from inhibitory to excitatory in *Shank3* KO mutants. In other words, the repetitive behaviors in *Shank3* KO mice resulted from a dysfunctional PrL-DMS pathway, which was functionally altered from promoting action switching to facilitating action repetition. This effect was further exacerbated by an excitatory, rather than inhibitory, interaction with the M1-DLS circuit (Fig. 8H).

Genetic restoration of *Shank3* in DMS but not DLS rescues sequence behavior

To verify that the awry PrL-DMS pathway is indeed the key mechanism underlying the repetitive behaviors in *Shank3* KO mice, we genetically restored *Shank3* expression in the striatum of these mutants and assessed their sequence behaviors. In the *Shank3* KO mice, AAV5-hsyn-mCherry-Cre was injected into DMS for genetic restoration of *Shank3* expression in the striatal subregion (fig. S7A and see Materials and Methods) (*47*). Notably, restoring *Shank3* expression in the DMS alone was sufficient to reduce excessive grooming in the *Shank3* KO mice (fig. S7B, yellow bar). These DMS *Shank3* restoration animals exhibited significant improvements during LLRR sequence learning and increased the efficiency through the 21 days of training (Fig. 9A; difference between littermate control and *Shank3* KO mice with DMS rescue: $F = 1.401$, $P = 0.26$; fig. S7C), with marked reduction in action repetition (fig. S7D). To assess changes in the D1/D2 ratio following *Shank3* restoration in the DMS, we conducted slice recordings of D1/D2-SPNs in DMS with optogenetic activation of PrL terminals. Compared to the *Shank3* KO mutants (Fig. 8, A and B), the DMS *Shank3* restoration animals showed increased EPSCs amplitude in both D1- and D2-SPNs (Fig. 9, B and C; EPSCs of D1-SPNs: 104.3 ± 17.8 pA, D2-SPNs: 148.9 ± 13.7 pA, $n = 8$ pairs; paired *t* test: PrL to D1-SPNs versus PrL to D2-SPNs, $P = 0.04$; unpaired *t* test, EPSCs from PrL to D1-SPNs between *Shank3* KO and *Shank3* KO with DMS rescue: $P = 0.028$, EPSCs from PrL to D2-SPNs between *Shank3* KO and *Shank3* KO with DMS rescue: $P < 0.0001$), highlighting restored synaptic physiology by *Shank3* expression (*47*). In the DMS *Shank3* restoration mice, the activation of PrL terminals induced larger EPSCs in the D2-SPNs than the D1-SPNs (Fig. 9, C and D), suggesting that the reversed D1/D2 ratio due to *Shank3* deletion (Fig. 8C) was rescued following *Shank3* restoration in the DMS (Fig. 9D; 0.72 ± 0.12, $n = 8$; unpaired *t* test, the D1/D2 ratio from PrL to DMS between *Shank3* KO and *Shank3* KO with DMS rescue: $P = 0.0008$; Fig. 5G; unpaired *t* test, the D1/D2 ratio from PrL to DMS between WT and *Shank3* KO with DMS rescue: $P = 0.88$).

Furthermore, we performed in vivo recording of M1 neurons ($n = 108$) with activating PrL terminals in DMS to examine the regulation effects of PrL-DMS pathway on M1 after *Shank3* restoration (Fig. 9E). Notably, we observed 18.5% of neurons showing inhibitory

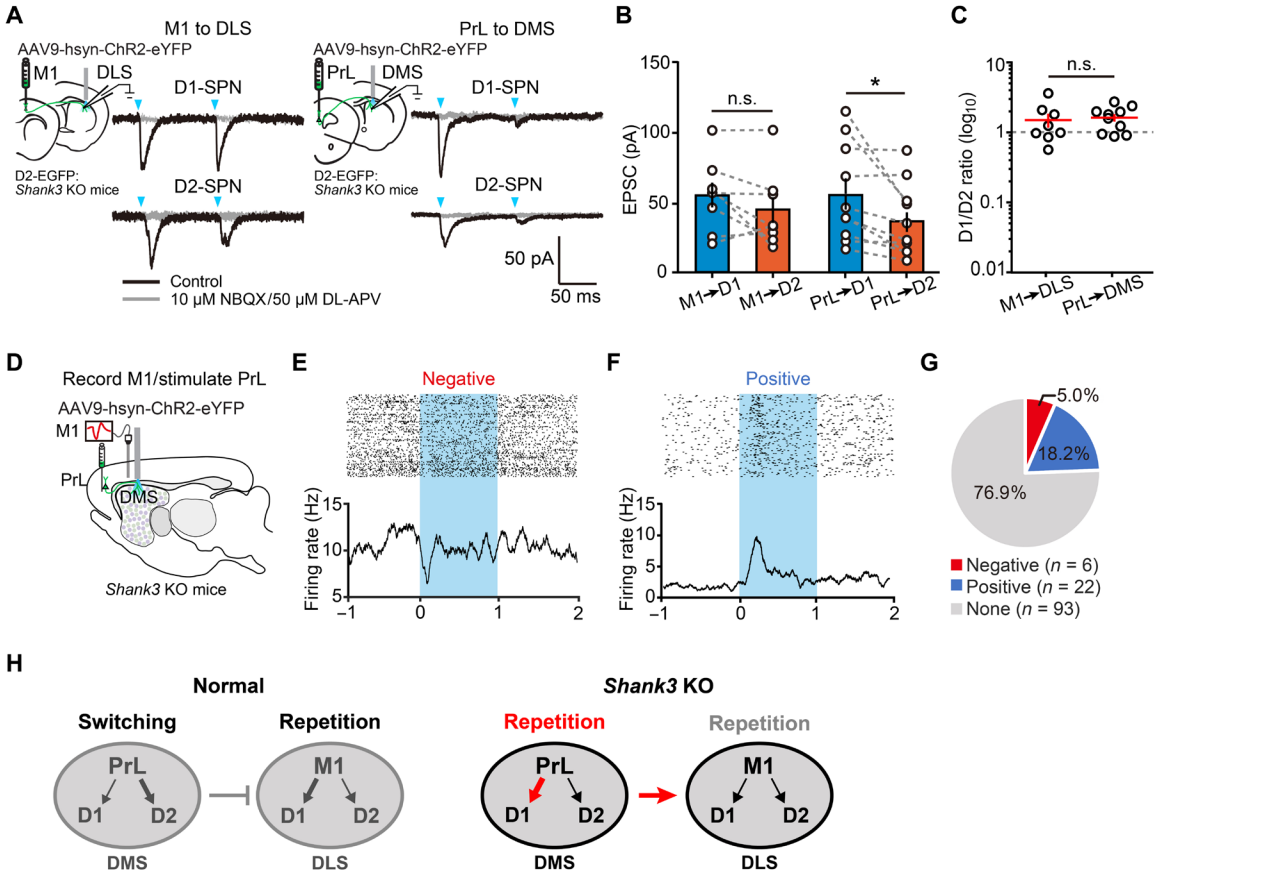

Fig. 8. Altered D1/D2 ratio in the PrL-DMS pathway and its modulatory effect on M1 in *Shank3* KO mice. (**A**) Example of evoked EPSCs in D1- and D2-SPNs in DLS when optogenetically activating M1 terminals in *Shank3* KO mice (left). Example of evoked EPSCs in D1- and D2-SPNs in DMS when activating PrL terminals in *Shank3* KO mice (right). (**B**) Left two bars: Statistics of evoked EPSCs in the D1- and D2-SPNs in DLS when activating M1 terminals in *Shank3* KO mice. Right two bars: Statistics of evoked EPSCs in the D1- and D2-SPNs in DMS when activating PrL terminals in *Shank3* KO mice. (**C**) Ratio of D1- and D2-SPNs evoked EPSCs in DLS when activating M1 terminals in *Shank3* KO mice (left) and in DMS when activating PrL terminals in *Shank3* KO mice (right). (**D**) Diagram of in vivo multi-unit recording of M1 when optogenetically stimulating PrL terminals in the DMS of *Shank3* KO mice. (**E** and **F**) Example of negative (E) and positive responsive neurons (F) in M1. (**G**) Pie chart indicating the proportion of negative responsive (red), positive responsive (blue), and nonresponsive M1 neurons (gray) when stimulating PrL terminals in the DMS of *Shank3* KO mice. (**H**) Diagram of the action sequencing model in WT mice (left) and in *Shank3* KO mice (right). In *Shank3* KO mice, function of the PrL-DMS pathway turns into regulating action repetition, mainly through the D1-SPNs. Stimulating the PrL-DMS pathway mainly activates M1 in this condition.

response (latency: 62.8 ± 1.8 ms) and 10.4% excitatory response in M1 (latency: 195.6 ± 9.8 ms) (Fig. 9, F to H). These percentages are significantly distinct from those in *Shank3* KO mice (Fig. 8G, two-proportion z test, negative response: $z = -3.4631$, $P < 0.001$; positive response: $z = 2.4369$, $P < 0.015$), suggesting that the main effect from the PrL-DMS pathway to M1 was restored to inhibitory after *Shank3* restoration in DMS. These results suggest that the inhibitory effect from the PrL-DMS pathway to M1 recovers after *Shank3* restoration in DMS. Moreover, optogenetic stimulation of DMS-projecting PrL neurons during the LLRR sequence task revealed that the action-switching function was also completely rescued in these DMS *Shank3* restoration animals (Fig. 9, J to R; $n = 6$, Wilcoxon matched-pairs signed rank test, length change under stimulation on the first left lever press, left: −0.36 ± 0.08, $P = 0.03$; right: −0.02 ± 0.04, $P = 0.88$; total: −0.37 ± 0.07, $P = 0.03$; length change under stimulation on the second left lever press, left: −0.11 ± 0.12, $P = 0.56$; right: 0.04 ± 0.06, $P = 0.69$; total: −0.07 ± 0.13, $P = 0.84$; length change under stimulation on the first right lever press, left: 0.23 ± 0.07, $P = 0.06$; right: −0.40 ± 0.09, $P = 0.03$; total: −0.17 ± 0.06, $P = 0.06$; length change under inhibition on the second right lever press, left: 0.20 ± 0.10, $P = 0.32$; right: −0.16 ± 0.07, $P = 0.06$; total: 0.04 ± 0.14, $P = 0.69$). In addition, we also performed similar set of experiments in *Shank3* KO mice by genetic restoration of *Shank3* expression in DLS. However, restoration of *Shank3* in the DLS failed to improve corticostriatal synaptic physiology, excessive grooming, sequence learning, and the action repetition/switching ratio (figs. S7 and S8). Together, these results suggest that restoring *Shank3* expression in the DMS, but not DLS, is sufficient to rescue the action switching function of PrL-DMS pathway and eliminate the repetitive behaviors in *Shank3* KO mice (Fig. 9S). Given the general implications of action switching in normal and pathological behaviors, these findings underscore the critical role of the frontostriatal circuitry in action control across various conditions.

DISCUSSION

In this study, by using a heterogeneous action sequence task that includes both action repetition and switching, we revealed two distinct yet complementary corticostriatal circuits crucial for performance of

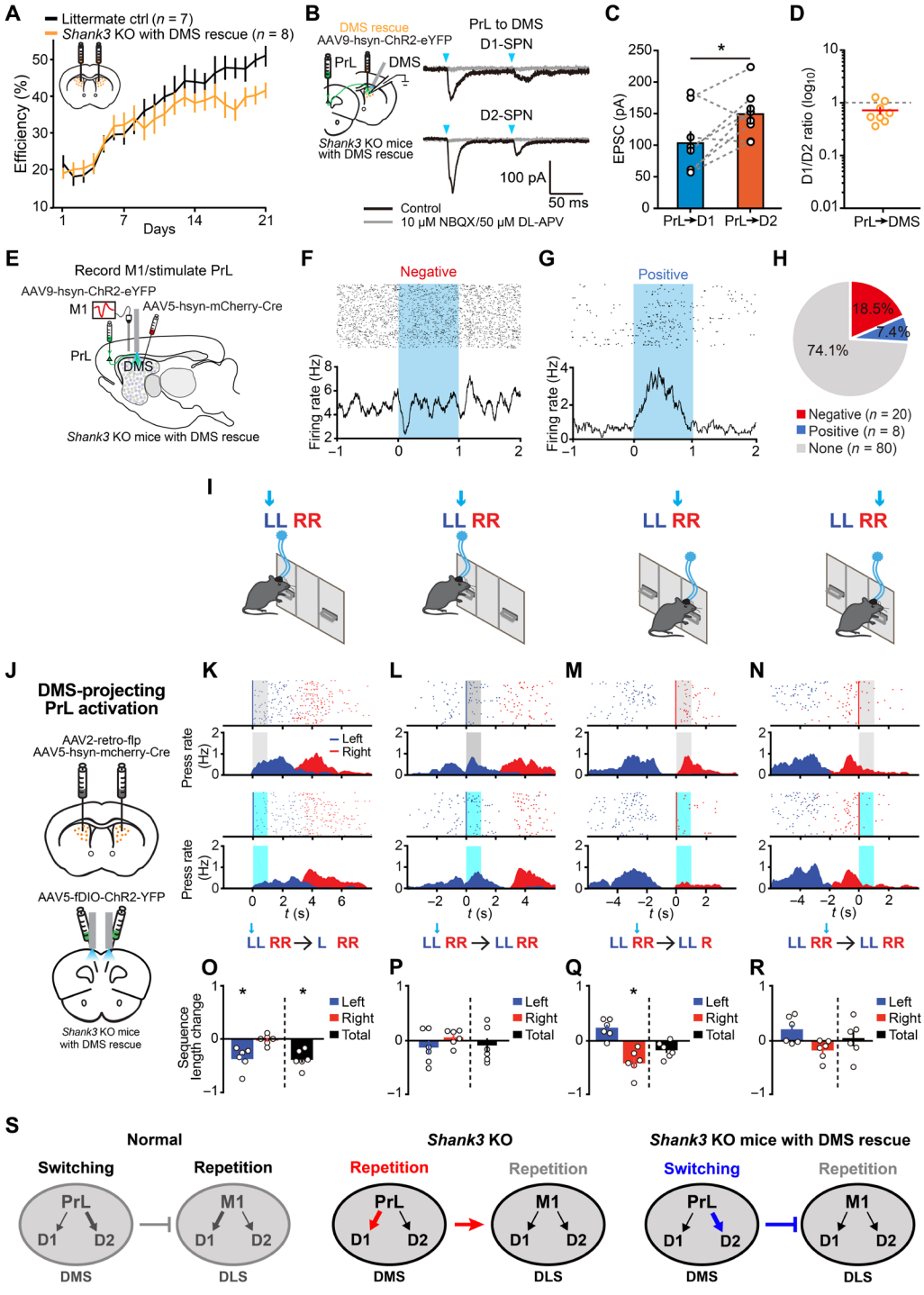

Fig. 9. Restoration of *Shank3* in DMS rescues the physiology and function of PrL-DMS pathway, as well as sequence behavior, in *Shank3* KO mice. (**A**) Learning curve of the LLRR sequence behavior in littermate ctrl (black) and *Shank3* KO mice with DMS rescue (yellow). (**B**) Example of evoked EPSCs in D1- and D2-SPNs in DMS during activation of PrL terminals in *Shank3* KO mice with DMS rescue. (**C**) Statistics of evoked EPSCs in the D1- and D2-SPNs during PrL terminal activation in *Shank3* KO mice with DMS rescue. (**D**) Ratio of D1- and D2-SPNs evoked EPSCs during activation of PrL terminals in *Shank3* KO mice with DMS rescue. (**E**) Diagram of in vivo multi-unit recording of M1 when stimulating PrL terminals in DMS of *Shank3* KO mice with DMS rescue. (**F** and **G**) Example of negative (F) and positive responsive neurons (G) in M1. (**H**) Pie chart showing the proportion of negatively (red), positively responsive (blue), and nonresponsive M1 neurons (gray). (**I**) Protocol for optogenetic experiment. (**J**) Diagram showing opto-activation of DMS-projecting PrL neurons in *Shank3* KO mice with DMS rescue. (**K** to **N**) Behavioral examples of striatal-projecting PrL neurons stimulation in *Shank3* KO mice with DMS rescue. (**O** to **R**) Sequence length change after DMS-projecting PrL neurons activation in *Shank3* KO mice with DMS rescue. (**S**) Diagram of action sequencing model in WT (left), *Shank3* KO (middle), and *Shank3* KO mice with DMS rescue (right). In *Shank3* KO mice with DMS rescue, activation of PrL-DMS pathway again triggers action switching through D2-SPNs. Stimulating PrL-DMS pathway mainly inhibits M1 under this condition.

action sequences. Specifically, the M1-DLS pathway regulates action repetition through its preferential innervations on striatal D1-SPNs, while the PrL-DMS pathway controls action switching via biased projections to striatal D2-SPNs. Because of a unidirectional inhibition from the PrL-DMS pathway to M1, the action switching mode takes precedence over the action repetition mode, forming a switching-repetition working model for action sequencing. In addition, in the *Shank3* KO mice, a genetic variant linked to ASD, the PrL-DMS circuit, has turned into an action repetition pathway due to awry corticostriatal synapses with biased projections from PrL to D1-SPNs. The unidirectional inhibition from PrL-DMS pathway to M1 was also altered to predominantly excitatory, further enhancing the action repetition mode and leading to the deficient sequence behaviors in these *Shank3* KO mutants. Notably, the genetic restoration of *Shank3* expression in DMS, but not in DLS, rescued the awry D1/D2 ratio in the PrL-DMS pathway, reinstated action switching function, and normalized the sequence behaviors and repetitive grooming. These results identify the specific corticostriatal circuits for action repetition and switching and unveil the dynamic interplay among corticostriatal pathways for controlling action selection in health and disease.

It has been suggested that learned action sequences are organized in a hierarchical manner (*20*), and previous studies showed striatal D1- and D2-SPNs control different hierarchies of behavior (*3*, *20*, *26*). At the sequence level, there are notably more striatal D1-SPNs than D2-SPNs signaling sequence start/stop. At subsequence and element levels, many striatal D1-SPNs exhibit sustained activity facilitating ongoing action when optogenetically activated, while striatal D2-SPNs mainly encode between-subsequence transition, triggering behavioral switches when stimulated (*20*). In this study, we found that there are a large proportion of M1 neurons encode sequence start/stop, implying a possibly critical role of M1 in sequence execution (*26*, *44*, *45*, *49*, *50*). While some reports suggest that M1 lesion has negligible effects on the execution of motor sequences (*51*, *52*), presumably due to the relatively simple structure of sequences studied, accumulating evidences show the impairment of action execution after lesion or silencing M1 (*43*, *44*, *50*, *53*–*55*). In the current study, we trained mice to perform a spatiotemporal heterogeneous LLRR action sequence including both action repetition and switching. Muscimol inactivation of M1 significantly reduced the sequence performance efficiency. Optogenetic silencing of M1 further demonstrated a reduction in lever pressing during the execution of learned action sequences, consistent with previous reports showing that photoinactivation of M1 leads to a cessation of behavior (*40*). Anatomically, M1 mainly projects to DLS (*36*, *56*). We also observed that many M1 neurons encode elemental actions with sustained firing activity during the LLRR sequence execution, similar to the striatal D1-SPNs in the same task (*20*). Our slice recordings revealed that M1 has targeted more strongly on striatal D1-SPNs than D2-SPNs, in line with previous reports (*45*, *57*). Prior studies have shown that this projection preference predominantly originates from pyramidal tract rather than telencephalic neurons (*46*). Optogenetic activation of the M1-DLS pathway, whether it is through stimulation of DLS-projecting M1 neuron soma or M1 neuronal terminals in DLS, facilitates ongoing actions, further establishing its role in regulating action repetition.

The prefrontal cortex (PFC) has long been known to play a critical role in many aspects of executive control, including action selection, action planning, and behavior flexibility (*42*, *58*–*63*). Our neuronal recordings revealed that, in addition to signaling sequence start/stop (*42*, *43*, *64*), a substantial proportion of PrL neurons specifically encode transitions between subsequences, suggesting a plausible role in controlling action switching. Consistently, learned LLRR sequence performance was markedly impaired following either pharmacological or optogenetic inactivation of the PrL, primarily due to deficits in action-switching behavior. These results suggest that PrL plays a critical role in controlling action switching, similar with the function of striatal indirect pathway D2-SPNs (*20*). As part of the limbic cortico-basal ganglia loop, PrL mainly projects to DMS (*36*, *56*). In contrast to the M1-DLS pathway, we found stronger synaptic projections from the PrL to striatal D2-SPNs than to D1-SPNs, suggesting that the PrL-DMS pathway controls action switching through biased innervation of striatal D2-SPNs. This was further confirmed by optogenetic stimulation of the PrL-DMS pathway during LLRR sequence execution. Again, whether it is by optogenetic excitation of DMS-projecting PrL neuron soma or PrL neuronal terminals in DMS, PrL-DMS pathway activation triggers action switching and facilitates the transition toward the next subsequence in the motor program.

Motor perseveration has long been recognized as a major behavioral sign following frontal lobe lesions (*65*). The PFC and associated cortico-basal ganglia circuitry have been demonstrated to be crucially involved in inhibiting inappropriate actions responding to either external cues or internal states (*66*–*69*). The current finding by identifying the critical role of PrL-DMS pathway in controlling action switching provides a fundamental principle to explain the functions of PFC in action selection, behavior flexibility, and inhibitory control. Furthermore, it has been previously shown that in rodents, the limbic cortico-basal ganglia-thalamocortical loop can unidirectionally influence the motor output through the nigrothalamic pathway (*36*). Our in vivo neuronal recording experiments found that optogenetic excitation of PrL-DMS pathway inhibits the M1 activity, but not vice versa, suggesting that the activation of action switching pathway suppresses action repetition circuit. This suppression likely arises from unidirectional regulation by the limbic system over motor output through the limbic striatum–medial substantia nigra (SNr)–motor thalamus–M1 circuitry, as previously described (*36*). Together, these results elucidate the cortiostriatal mechanisms underlying action repetition and switching and establish the logic and interaction for two functionally distinct circuits that control action sequencing in the healthy brain.

In many neurological and psychiatric conditions, such as ASD and OCD, repetitive behavior is one of the most prominent symptoms, where altered corticostriatal circuits have been generally found (*30*–*33*, *47*), such as the anterior cingulate cortex (ACC), orbitofrontal cortex (OFC), and PFC to striatum circuits (*70*–*73*). Recent studies have shown that dysfunction of the ACC is associated with social deficits but not repetitive grooming (*74*). OFC with its major projections to the central striatum has been demonstrated involving in grooming in both WT and *Sapap3* mutant mice (*71*, *72*). As a prevailing theory based on the cortico-basal ganglia circuit in the OCD pathology, formation of compulsive repetitive behavior is a shift from normal goal-directed behaviors to pathological habits (*75*). Considering the function of DLS and DMS in habitual and goal-directed behaviors (*76*, *77*), in our study, we approached the mechanism underlying repetitive behavior through focusing on M1 and PrL with their dense projections to DLS and DMS, respectively. Previous studies on repetitive behaviors in

animal models of neurological or psychiatric disorders mostly focus on innate behaviors such as grooming, jumping, circling, or marble burying (*30*, *32*, *33*, *70*, *71*). However, many repetitive behaviors of ASD or OCD conditions are learned, such as various acquired ritual behaviors composed of stereotyped action sequences (*16*, *17*, *72*). Therefore, the LLRR action sequence task used in current study including both action repetition and switching components provides an ideal framework to study the circuit mechanism underlying pathological repetitive behaviors in disease brains.

Shank3 KO mice as a genetic animal model for ASD has both the deficits of social interaction and stereotyped repetitive behavior such as overgrooming (*33*, *47*). In the current study, besides excessive grooming, we found severe deficits in learning and performance of LLRR action sequences, with nearly doubled action repetition/switching ratio in the *Shank3* KO mice compared to their littermate controls. On the basis of our findings in healthy brain, where the M1-DLS pathway mediates action repetition and the PrL-DMS circuit controls action switching, one might hypothesize either enhanced repetition or diminished switching pathway underlying the ASD symptoms in the *Shank3* KO mice. In contrast with the WT animals, it was found that optogenetic activation of the M1-DLS pathway had negligible effects on learned sequence behavior, while activation of the PrL-DMS pathway caused action repetition in *Shank3* KO mice. These findings suggest a corticostriatal mechanisms underlying action sequence deficiency in *Shank3* KO mice, in which the original action switching pathway has turned into an action repetition pathway, leading to the impaired action switching and repetitive behaviors.

Our followed slice electrophysiology experiments reveal reduced corticostriatal excitatory synaptic transmission at both the M1-DLS and PrL-DMS pathways in *Shank3* KO mice, consistent with previous studies (*34*). Notably, it was found that the D1/D2 ratio was reversed in the PrL-DMS pathway, which turns from the action switching to action repetition function and led to impaired action switching in these *Shank3* KO mutants. In addition, the dominant inhibitory effect of the PrL-DMS pathway on M1 observed in WT mice, became excitatory in *Shank3* KO mice, further deteriorating the interplay between the PrL-DMS and M1-DLS pathways and the action switching function in *Shank3* KO mice. Together, these results have pinpointed the critical contribution of impaired action switching associated with awry PrL-DMS circuit underlying repetitive behaviors in *Shank3* KO mice. Therefore, after genetic restoration of *Shank3* expression in DMS but not in DLS of *Shank3* KO mice, we found it recovered the D1/D2 ratio in the PrL-DMS pathway, which in turns rescued the action switching function and the sequence behavior. It is noteworthy that both excessive grooming and repetitive lever pressing were notably diminished in the DMS *Shank3* rescued mice, suggesting a universal action switching function of the PrL-DMS circuit for controlling both innate and learned action sequences.

MATERIALS AND METHODS

Mice

All procedures were approved by the Animal Advisory Committee at East China Normal University and the Salk Institute Animal Care and Use Committee (Salk IACUC 12-00032) and were conducted in accordance with the National Institutes of Health Guidelines for the Care and Use of Laboratory Animals. Experiments involved both male and female mice, all of which were housed on a 12-hour light/12-hour dark cycle. WT (C57BL/6), $Vgat^{Cre/+}$:Ai32, $Shank3^{fx/fx}$ (*Shank3* KO, RRID:IMSR_JAX:028800) (*33*), $Shank3^{fx/+}$ (*Shank3* heterozygous), and $Shank3^{+/+}$ (*Shank3* littermate control) mice were used for behavior experiments. $Vgat^{Cre/+}$:Ai32 mice were crossed from $Vgat^{Cre/+}$ (RRID:IMSR_JAX:016962) and Ai32 mice (RRID:IMSR_JAX:024109). For in vivo recording, WT and *Shank3* KO mice were used to record M1 and PrL neurons. For slice recording, D2-EGFP (RRID: MMRRC_000230-UNC) and D1-Cre mice (RRID: MMRRC_034258-UCD) with AAV5-flex-mCherry injection were used to identify D2-SPNs and D1-SPNs under the WT background, respectively; only *Shank3* KO:D2-EGFP mice were used to identify D1- versus D2-SPNs under the *Shank3* KO background.

Behavioral training and quantification

Both the continuous reinforcement (CRF) and LLRR sequence tasks are the same as previous report (*20*). Behavior experiments were conducted inside a sound-attenuating box (Med Associates operant chamber, Med Associates, catalog no. MED-307 W-D1), where an operant chamber was equipped with a food magazine that had an infrared beam to record each magazine entry, a house light (3 W, 24 V) on the opposite side of the magazine and two retractable levers placed on each side of the house light. A food pellets dispenser connected to the food magazine would deliver a pellet whenever the mouse finished certain lever press. Behavioral chamber was controlled by the behavioral software (MED-PC IV, Med Associates, VT) that recorded all time stamps of lever presses and magazine entries with a resolution of 10 ms. All behavioral programs were custom-written.

Before behavioral training, mice were food-restricted and then were given 2 g of normal chow per day to maintain their body weight at ~85% of their original weight. Training began with the CRF, as described previously (*20*, *26*). The CRF procedure initiated with the illumination of the house light and the extension of either left or right lever. Mice typically went through 3 days of CRF with receiving reinforcers up to 5, 10, and 15 within 1 hour per session on day 1, day 2, and day 3, respectively. Each day featured two consecutive sessions where either the left or right lever was extended randomly. Mice that failed to obtain 15 pellets on the third day continued daily 15-pellet per session testing until they successfully completed the task within 1 hour per session.

Once finished CRF, mice continue to be trained on the LLRR sequence task. The LLRR task started with the illumination of the house light and the extension of both the left and right levers simultaneously. During training, both levers will not retract and are always available for pressing. Mice received reinforcers delivered to the food magazine whenever they pressed the lever as the consecutive LLRR pattern. Within one trial, extra lever presses besides the LLRR pattern did not exclude the reward. One training session would be ended once mice received 40 reinforcers or the session lasted for 120 min.

For behavioral quantification, the initiation of a sequence was defined as the first lever press following the last magazine entry. Sequence termination was determined either by the magazine entry at the end of a rewarding trial or by the end of the right subsequence in nonrewarding trials. The termination of the left or right subsequence was determined by the distribution of interpress intervals (IPIs) of each mouse. The IPIs distributed as multimodal because there were the shortest intervals (within subsequence), shorter

intervals (switching between subsequences), and longer intervals (sequences separated by magazine checking). The left and right subsequences were identified as the first peak in the IPI distribution (*26*, *41*). For groups undergoing optogenetic manipulation, all data went through an additional post hoc analysis process to better identify discrete sequences. Behavior efficiency was calculated as the percentage of rewarded lever presses (LLRR, four presses per reward) relative to the total number of presses during a session (*20*).

Surgery and implantation

Mice were anesthetized with either isoflurane (4% induction, 1 to 2% sustained) or a cocktail of ketamine (100 mg/kg) and xylazine (10 mg/kg). The head was shaved and placed in a Kopf stereotaxic frame. The scalp was cleaned with 70% ethanol and povidone iodine. Subsequently, bupivacaine was subcutaneously injected for local anesthesia before the incision. After opening the scalp, the skull was cleaned and leveled at bregma and lambda, and a mounted drill was used to create holes in the skull.

For muscimol infusion, a 26-gauge bilateral guide cannula (Plastics One, VA) with 3.0-mm center-to-center distance was implanted into M1 following the coordinates: +1.1 mm anterior-posterior (AP), ±1.5-mm medio-lateral (ML), −0.9-mm dorso-ventral (DV). A 26-gauge bilateral guide cannula (Plastics One, VA) with 0.8-mm center to center distance was implanted into PrL following the coordinates: +2.0-mm AP, ±0.4-mm ML, −1.6-mm DV. Dummy cannulas fitted to the length of the guide cannulas were inserted after surgery.

For virus injection, a Hamilton syringe was used to inject 200 nl of AAV5-fDIO-ChR2(H134R)-YFP (University of North Carolina Vector Core) or AAV9-flex-GFP (Salk GT3 Core) into either M1 or PrL area using following coordinates: +1.1-mm AP, ±1.6-mm ML, −0.9-mm DV for M1; +2.0-mm AP, ±0.4-mm ML, −1.6-mm DV for PrL. A total of 750 nl of AAV2-retro-flp (Salk GT3 Core), AAV5-retro-Cre (Salk GT3 Core), AAV5-flex-mCherry (Salk GT3 Core), and AAV5-hsyn-mCherry-Cre (University of North Carolina Vector Core) were injected into DLS or DMS using following coordinates: +0.2-mm AP, ±2.5-mm ML, −2.7-mm DV for DLS; +0.5-mm AP, ±1.5-mm ML, −2.5-mm DV for DMS. After positioning at the injection site, the syringe was held in place for 5 min before starting the injection. The injection speed was maintained at 100 nl/60 s. Following injection, the syringe was left in place for at least 5 min before withdraw.

For fiber implantation, optic fibers (200 μm, 0.37 numerical aperture) were constructed as previously described (*20*). For PrL, optic fibers were implanted at a 10° angle to allow sufficient space for bilateral fibers using following coordinates: +2.0-mm AP, ±0.9-mm ML, −1.1-mm DV. For mediodorsal thalamus (MD), optic fibers were implanted at a 15° angle to ensure enough space for bilateral fibers using following coordinates: −1.2-mm AP, ±1.3-mm ML, −2.8-mm DV. For others area, optic fibers were implanted as following coordinates: M1: +1.1-mm AP, ±1.6-mm ML, −0.4-mm DV; DLS: +0.2-mm AP, ±2.5-mm ML, −2.3-mm DV; DMS: +0.5-mm AP, ±1.5-mm ML, −2.1-mm DV; CLA: +1.0-mm AP, ±2.75-mm ML, −2.5-mm DV; Amy: −1.6-mm AP, ±3.4-mm ML, −4.2-mm DV.

Implantation of electrode array (Innovative Neurophysiology) for in vivo recording was performed as described previously (*26*, *27*). The electrode arrays used in this study contained 16 tungsten contacts (2 × 8), each 35 μm in diameter and 5 mm in length. Electrodes were spaced 150 mm apart in the same row and 200 mm apart between two rows (Innovative Neurophysiology Inc., NC). Arrays were placed randomly in either side of hemisphere toward the AP position with the center targeting following coordinates: +1.1-mm AP, ±1.6-mm ML, −0.9-mm DV for M1; +2.0-mm AP, ±0.4-mm ML, −1.6-mm DV for PrL. The silver grounding wire was attached to the skull screw. After implantations, cannulas, optic fibers or electrode arrays were fixed to skull using the dental acrylic (Contemporary Ortho-Jet powder and liquid, Lang Dental, IL). After surgery, mice received buprenorphine (0.5 to 1 mg/kg) for analgesic and were allowed to recover for at least 1 week in their home cages before food restriction and behavioral training.

Muscimol experiments

Following cannulas implantation, mice were retrained to achieve at least 40% behavioral efficiency before muscimol infusion. Over the next three consecutive days, mice underwent infusions of saline, muscimol (0.05 μg/μl; Sigma-Aldrich), and saline, respectively. Before infusion, mice were briefly anesthetized using isoflurane and injection cannulas (Plastics One, VA) were bilaterally inserted into the cannulas. Subsequently, 200 nl of saline or muscimol was slowly infused into the target area using an infusion pump (BASi, IN) connected to two syringes containing infusion liquid and linked to the injection cannulas via polyethylene tubing. After infusion, the injection cannulas were left in place for 5 min before removal. Mice were then returned to their home cage and rested for 30 min before starting behavior task. Behavioral sessions ended until mice received 40 reinforcers or lasted for 120 min.

Optogenetic experiments

Following optic fiber implantation, mice were retrained while tethered via fiber optic cables connecting optrode ferrules to a commutator (Doric, Canada) to allow free rotation within the behavioral chamber. Optogenetic stimulation began once behavior efficiency reached above 40%. Here, we defined four stimulation conditions based on the four lever presses of the LLRR sequence: the first (left), second (left), third (right), or fourth (right) lever press triggered 1-s stimulation on each condition. The stimulation was delivered by a 473-nm laser (Laserglow Technologies, Canada) triggered by a Transistor-Transistor Logic (TTL) output programmed in the behavioral software (MED-PC IV, Med Associates, VT). Mice underwent one stimulation condition per day, with half of the randomized trials receiving stimulation and the rest trials as control. The stimulation session ends after mice received 80 reinforcers or lasted for 180 min. The change in lever press length of each mouse was calculated by subtracting the values of stimulated trials from those of nonstimulation trials within the same session. Sometimes stimulation conditions were repeated across multiple days to ensure enough trials for analysis (*20*). Stimulation effects were compared through the perievent time histograms (PETHs) between control and stimulated sequences. All lever presses were aligned to the stimulated press, averaged in 100-ms bins, and filtered with a Gaussian low-pass filter (window size = 5, SD = 5). PETHs were plotted while excluding the referenced lever press to avoid misleading results caused by the narrow smoothing window artificially inflating lever press rates. Other stimulation pattern, such as 200-ms and 10-ms light pulses delivered at 14 Hz for 1 s, was used to demonstrate the consistency of stimulation effects across different stimulation parameters.

In vivo recording during sequence performance

In vivo recording of M1 and PrL neurons while mice are doing the task was performed as previously described (*20*, *26*, *41*). Following

electrode implantation, mice were retrained while tethered via a recording cable connecting electrode to the amplifier. Recording started after mice reached 40% efficiency to ensure stable behavior performance. Neural activity was recorded using the MAP system (Plexon Inc., Dallas, TX). Behavior data including time stamps of lever presses and magazine entries were recorded simultaneously by the behavioral software (MED-PC IV, Med Associates, VT). Spikes were initially sorted online used a built-in algorithm (Plexon Inc., Dallas, TX). Only those with stereotypical waveforms were tagged and saved. After recording, spikes were further sorted into individual units using the offline sorting software (Offline Sorter, Plexon Inc., Dallas, TX). Identified units had no spikes during the refractory period (larger than 1.3 ms).

For the LLRR task, neuronal activity was aligned to the first left, final left, first right, or final right lever press, averaged across all trials in 10-ms bins, and smoothed using a Gaussian filter low-pass filter (window size = 5, SD = 5) to construct PETH. Neuronal activity between mice leaving the magazine and initiating lever pressing of next trial was sampled with a 10-s time window 50 times as the baseline activity for each unit. Baseline activity was averaged across all 50 samples, binned with 10-ms time bins, and filtered with the same Gaussian filter mentioned above. Neuronal activity with 10-ms time bins, occurring 1000 ms before and after each lever press, was used to determine the significance of sequence-related activity (*20*, *26*, *41*). Activity was significant when at least five consecutive bins of firing rate increasing more than 95% (2 × SD) of the baseline activity or decreasing below 68% (1 × SD) of the baseline activity within 500 ms before and after lever press (*20*, *26*, *41*).

Sequence start/stop related neurons were those with a significant firing rate modulation before the first left press (start) and/or after the final right press (stop) of the sequence. This modulation was significantly larger than other firing rate modulations associated with remaining presses within the sequence. Switching-related neurons were defined as those exhibiting significant firing rate modulation during the transition period, relative to baseline activity. Sustained or inhibited activity was defined as a significant positive or negative firing rate modulation constantly associated with multiple lever presses in the sequence (*20*, *26*, *41*). All analyses were performed using custom-written scripts in MATLAB (MathWorks, MA).

In vivo acute recording with opto-stimulation

In vivo acute recording of M1 or PrL neurons during optogenetic stimulation was performed as previously described (*36*). Briefly, AAV9-hsyn-ChR2-eYFP (Salk GT3 Core) was injected into M1 or PrL of WT mice. After 3 weeks of virus injection, mice were anesthetized under isoflurane (4% induction, 1 to 2% sustained) and immobilized with four limbs and tail fixed on the plate. The remaining steps followed the electrode implantation procedure (see above), except that dental cement was not applied to fix the electrode to the skull. Before lowering the electrode into the brain, optic fiber was placed into DLS for M1 terminals stimulation or DMS for PrL terminals stimulation. The silver grounding wire of the electrode was attached to the skull screw. Then, electrode was gradually lowered into PrL or M1. Once the electrode reached the surface layer of M1 or PrL, the isoflurane was cut off and waited for the mice to fully awake. After that, the electrode was lowered incrementally, enabling the recording of neurons at multiple depths in each cortical area.

When recording started, blue laser stimulation (3 to 4 mw) was delivered through the optic fiber via a fiber-optic patch cord connecting to a 473-nm laser. Three stimulation patterns including 1-s constant light, 5 Hz, and 20 Hz (10-ms pulse duration) were delivered randomly during recording. The intertrial interval was 4 s, and each pattern was repeated ~50 trials. Neuronal activity was aligned to the stimulation onset at 0, averaged in 5-ms time bins, and smoothed using a Gaussian filter low-pass filter. Neuronal activity during the 1 s before stimulation onset was used as baseline activity. Neurons were classified as responsive to stimulation if their firing rate during the stimulation period increased by more than 3 × SD of baseline activity or decreased below 1 × SD of baseline activity. The latency was measured by the time when neuron firing rate first reached the criterion above.

Slice recording

Slice recording of D1- and D2-SPNs while giving optogenetic stimulation was performed as previously described (*36*). Briefly, 4 weeks before recording, AAV9-hsyn-ChR2-eYFP was injected into both side of M1 or PrL of D2-EGFP, D2-EGFP:*Shank3* KO, or D1-Cre:*Shank3* KO mice with injection of AAV5-flex-mCherry in dorsal striatum. Before slice recording, mice were anesthetized using ketamine (100 mg/kg) and xyzaline (10 mg/kg) cocktail and transcardially perfused with ice-cold NMDG cutting solution (saturated with 95% O_2/5% CO_2) contained the following: 105 mM NMDG, 105 mM HCl, 2.5 mM KCl, 1.2 mM NaH_2PO_4, 26 mM $NaHCO_3$, 25 mM glucose, 5 mM sodium L-ascorbate, 3 mM sodium pyruvate, 2 mM thiourea, 10 mM $MgSO_4$, and 0.5 mM $CaCl_2$ (300 mOsm/kg, pH = 7.4). Then, the fresh brains were cut into coronal slice of 300-μm thickness under the ice-cold NMDG cutting solution by a vibratome (Leica VT1000S). Brain slices were incubated in 33°C NMDG cutting solution for 15 min and then transferred to 27°C normal artificial cerebrospinal fluid (ACSF) containing: 125 mM NaCl, 2.5 mM KCl, 1.25 mM NaH_2PO_4, 25 mM $NaHCO_3$, 12.5 mM D-glucose, 1 mM $MgCl_2$, and 2 mM $CaCl_2$ (295 mOsm/kg, pH = 7.4) for 45-min recovery. Both 33°C NMDG cutting solution and 27°C normal ACSF were bubbled with 95% O_2/5% CO_2. After that, slice was transferred to the recording chamber with ACSF bubbled with 95% O_2/5% CO_2 perfused at ~2 ml/min.

Whole-cell recording was performed under a 40× objective lens. D1- and D2-SPNs were identified through the fluorescence expression. Recording micropipettes (BF100-58-10, Sutter Instrument) were pulled by a Sutter P-97 puller with the resistance of 5 megohm, filled with internal solution containing: 115 mM KCl, 10 mM Hepes, 1 mM EGTA, and 12 mM tetraethylammonium chloride, 5 mM QX-314 (Br− salt), 4 mM MgATP, 0.3 mM Na–guanosine 5′-triphosphate, and 8 mM Na_2-phosphocreatine (pH 7.3 adjusted with KOH; 295 mOsm/kg). After breaking in, cells were held at −70 mV for recording. The paired pulses light stimulation (473 nm, 5 to 60 mW/mm^2, 0.05 Hz, 2.5 ms, 50-ms ISI) were delivered by a 473-nm blue Diode-Pumped Solid-State (DPSS) laser system (Laserglow Technologies, Canada) through a 200-μm optic fiber (ThorLabs) positioned close to the patched cell (~50 to 150 μm) to evoked EPSCs. After recording 20 control trials (trial duration of 10 s), ACSF with 10 mM 6-cyano-7-nitroquinoxaline-2,3-dione (Tocris) and 50 mM DL-APV (Sigma-Aldrich) was perfused into the recording chamber to inhibit AMPA receptor– and NMDA receptor–mediated excitatory currents and recorded for another 20 trials. Access or series resistance ranged from <20 megohm and was monitored online. Any changes greater than 20% were excluded from the analysis. Data acquisition and signal processing were made with a patch-clamp amplifier (MultiClamp 700A, Axon Instruments) and Digidata (1440A, Axon Instruments), and all signals were

filtered at 3 kHz and sampled at 10 kHz using Clampex 10.1 (Molecular Devices). In D2-EGFP mice, D2-SPNs were identified by EGFP fluorescent, while paired D1-SPNs were selected on the basis of comparable soma size and lack of fluorescence within a 30-μm radius of the identified D2-SPNs. Similarly, in D1-Cre mice injected with AAV5-flex-mCherry, the same approach was used to select D1-SPNs and paired D2-SPNs.

Shank3 rescue experiments

For *Shank3* rescue experiments, 750 nl of AAV5-hsyn-mCherry-Cre was bilaterally injected into either DMS or DLS of *Shank3* KO mice at the age of 8 weeks. As the rescue of *Shank3* reported previously (*47*), all behavioral and electrophysiological experiments were conducted at least 6 weeks after *Cre* injection. For opto-stimulation and acute recording experiments, virus [AAV2-retro-flp, AAV5-fDIO-ChR2(H134R)-YFP, and AAV9-hsyn-ChR2-eYFP] injection with or without optic fiber implantation were done 4 weeks after *Cre* injection. With at least another 2 weeks' recovery, mice were used for later optogenetic or acute recording experiments. Grooming behavior was assessed as previously described (*47*). Mice were videotaped in their home cage from 19:00 to 21:00. Instances such as face-wiping, scratching/rubbing of head, ears, back, limbs and tails were all treated as grooming behavior.

Statistics

Learning data in WT mice were analyzed using one-way ANOVA. Learning data in littermate control, *Shank3* het, *Shank3* KO, *Shank3* KO with DLS rescue, and *Shank3* KO with DMS rescue were compared using one-way ANOVA with Tukey's multiple comparison test. Repetition versus switching ratio and grooming percentage were also analyzed through one-way ANOVA with Tukey's multiple comparison test. Optogenetic data were analyzed on the basis of control and stimulated values for each mouse per stimulation condition. The Wilcoxon matched-pairs signed rank test was used for this analysis. In vivo neuronal recording data were analyzed using two-sample z test for the comparison of proportions. Slice recording data were compared to either paired or unpaired t test. All data were initially analyzed in MATLAB (MathWorks, MA), and all statistics were performed using GraphPad Prism 7 (GraphPad Software, CA). Results are presented as means ± SEM except for the neuronal recording data, which are presented as percentages of the task-related positively identified units. $P < 0.05$ was considered significant.

Supplementary Materials

This PDF file includes:

Figs. S1 to S8

REFERENCES AND NOTES

1. K. Lasley, The problem of serial order in behavior, in *Cerebral Mechanisms in Behavior,* L. A. Jeffress, Ed. (Wiley, 1951), pp. 112–146.
2. C. R. Gallistel, *The organization of action: A new synthesis.* (Psychology Press, 2013).
3. X. Jin, R. M. Costa, Shaping action sequences in basal ganglia circuits. *Curr. Opin. Neurobiol.* **33**, 188–196 (2015).
4. S. Grillner, B. Robertson, The basal ganglia over 500 million years. *Curr. Biol.* **26**, R1088–R1100 (2016).
5. M. S. Brainard, A. J. Doupe, What songbirds teach us about learning. *Nature* **417**, 351–358 (2002).
6. A. M. Graybiel, The basal ganglia and chunking of action repertoires. *Neurobiol. Learn. Mem.* **70**, 119–136 (1998).
7. O. Hikosaka, H. Nakahara, M. K. Rand, K. Sakai, X. Lu, K. Nakamura, S. Miyachi, K. Doya, Parallel neural networks for learning sequential procedures. *Trends Neurosci.* **22**, 464–471 (1999).
8. R. Benecke, J. C. Rothwell, J. P. Dick, B. L. Day, C. D. Marsden, Disturbance of sequential movements in patients with Parkinson's disease. *Brain* **110**, 361–379 (1987).
9. D. Craufurd, J. C. Thompson, J. S. Snowden, Behavioral changes in Huntington disease. *Cogn. Behav. Neurol.* **14**, 219–226 (2001).
10. S. L. Rauch, C. R. Savage, N. M. Alpert, D. Dougherty, A. Kendrick, T. Curran, H. D. Brown, P. Manzo, A. J. Fischman, M. A. Jenike, Probing striatal function in obsessive-compulsive disorder: A PET study of implicit sequence learning. *J. Neuropsychiatry Clin. Neurosci.* **9**, 568–573 (1997).
11. K. C. Berridge, J. W. Aldridge, K. R. Houchard, X. Zhuang, Sequential super-stereotypy of an instinctive fixed action pattern in hyper-dopaminergic mutant mice: A model of obsessive compulsive disorder and Tourette's. *BMC Biol.* **3**, 4 (2005).
12. W. X. Chmielewski, C. Beste, Action control processes in autism spectrum disorder—Insights from a neurobiological and neuroanatomical perspective. *Prog. Neurobiol.* **124**, 49–83 (2015).
13. M. Oosterloo, D. Craufurd, H. Nijsten, E. van Duijn, Obsessive-compulsive and perseverative behaviors in Huntington's disease. *J. Huntingtons Dis.* **8**, 1–7 (2019).
14. E. C. Miguel, B. J. Coffey, L. Baer, C. R. Savage, S. L. Rauch, M. A. Jenike, Phenomenology of intentional repetitive behaviors in obsessive-compulsive disorder and Tourette's disorder. *J. Clin. Psychiatry* **56**, 246–255 (1995).
15. D. J. Stein, D. L. C. Costa, C. Lochner, E. C. Miguel, Y. C. J. Reddy, R. G. Shavitt, O. A. van den Heuvel, H. B. Simpson, Obsessive–Compulsive disorder. *Nat. Rev. Dis. Primers* **5**, 52 (2019).
16. M. Turner, Repetitive behaviour in autism: A review of psychological research. *J. Child Psychol. Psychiatry* **40**, 839–849 (1999).
17. S. R. Leekam, M. R. Prior, M. Uljarevic, Restricted and repetitive behaviors in autism spectrum disorders: A review of research in the last decade. *Psychol. Bull.* **137**, 562–593 (2011).
18. S. E. Halliday, D. A. Winter, J. S. Frank, A. E. Patla, F. Prince, The initiation of gait in young, elderly, and Parkinson's disease subjects. *Gait Posture* **8**, 8–14 (1998).
19. C. A. Bloxham, T. A. Mindel, C. D. Frith, Initiation and execution of predictable and unpredictable movements in Parkinson's disease. *Brain* **107**, 371–384 (1984).
20. C. E. Geddes, H. Li, X. Jin, Optogenetic editing reveals the hierarchical organization of learned action sequences. *Cell* **174**, 32–43.e15 (2018).
21. M. E. Franklin, E. B. Foa, Treatment of obsessive compulsive disorder. *Annu. Rev. Clin. Psychol.* **7**, 229–243 (2011).
22. A. Masi, M. M. DeMayo, N. Glozier, A. J. Guastella, An overview of autism spectrum disorder, heterogeneity and treatment options. *Neurosci. Bull.* **33**, 183–193 (2017).
23. X. Yu, Z. Qiu, D. Zhang, Recent research progress in autism spectrum disorder. *Neurosci. Bull.* **33**, 125–129 (2017).
24. R. L. Albin, A. B. Young, J. B. Penney, The functional anatomy of basal ganglia disorders. *Trends Neurosci.* **12**, 366–375 (1989).
25. M. R. DeLong, Primate models of movement disorders of basal ganglia origin. *Trends Neurosci.* **13**, 281–285 (1990).
26. X. Jin, F. Tecuapetla, R. M. Costa, Basal ganglia subcircuits distinctively encode the parsing and concatenation of action sequences. *Nat. Neurosci.* **17**, 423–430 (2014).
27. H. Li, X. Jin, Multiple dynamic interactions from basal ganglia direct and indirect pathways mediate action selection. *eLife* **12**, RP87644 (2023).
28. J. B. Smith, J. R. Klug, D. L. Ross, C. D. Howard, N. G. Hollon, V. I. Ko, H. Hoffman, E. M. Callaway, C. R. Gerfen, X. Jin, Genetic-based dissection unveils the inputs and outputs of striatal patch and matrix compartments. *Neuron* **91**, 1069–1084 (2016).
29. N. R. Wall, M. De La Parra, E. M. Callaway, A. C. Kreitzer, Differential innervation of direct- and indirect-pathway striatal projection neurons. *Neuron* **79**, 347–360 (2013).
30. J. M. Welch, J. Lu, R. M. Rodriguiz, N. C. Trotta, J. Peca, J.-D. Ding, C. Feliciano, M. Chen, J. P. Adams, J. Luo, S. M. Dudek, R. J. Weinberg, N. Calakos, W. C. Wetsel, G. Feng, Cortico-striatal synaptic defects and OCD-like behaviours in *Sapap3*-mutant mice. *Nature* **448**, 894–900 (2007).
31. Y. Wan, K. K. Ade, Z. Caffall, M. I. Ozlu, C. Eroglu, G. Feng, N. Calakos, Circuit-selective striatal synaptic dysfunction in the *Sapap3* knockout mouse model of obsessive-compulsive disorder. *Biol. Psychiatry* **75**, 623–630 (2014).
32. S. V. Shmelkov, A. Hormigo, D. Jing, C. C. Proenca, K. G. Bath, T. Milde, E. Shmelkov, J. S. Kushner, M. Baljevic, I. Dincheva, A. J. Murphy, D. M. Valenzuela, N. W. Gale, G. D. Yancopoulos, I. Ninan, F. S. Lee, S. Rafii, Slitrk5 deficiency impairs corticostriatal circuitry and leads to obsessive-compulsive-like behaviors in mice. *Nat. Med.* **16**, 598–602 (2010).
33. J. Peça, C. Feliciano, J. T. Ting, W. Wang, M. F. Wells, T. N. Venkatraman, C. D. Lascola, Z. Fu, G. Feng, *Shank3* mutant mice display autistic-like behaviours and striatal dysfunction. *Nature* **472**, 437–442 (2011).
34. W. Wang, C. Li, Q. Chen, M. S. van der Goes, J. Hawrot, A. Y. Yao, X. Gao, C. Lu, Y. Zang, Q. Zhang, K. Lyman, D. Wang, B. Guo, S. Wu, C. R. Gerfen, Z. Fu, G. Feng, Striatopallidal

dysfunction underlies repetitive behavior in *Shank3*-deficient model of autism. *J. Clin. Invest.* **127**, 1978–1990 (2017).
35. G. E. Alexander, M. R. DeLong, P. L. Strick, Parallel organization of functionally segregated circuits linking basal ganglia and cortex. *Annu. Rev. Neurosci.* **9**, 357–381 (1986).
36. S. Aoki, J. B. Smith, H. Li, X. Yan, M. Igarashi, P. Coulon, J. R. Wickens, T. J. Ruigrok, X. Jin, An open cortico-basal ganglia loop allows limbic control over motor output via the nigrothalamic pathway. *eLife* **8**, e49995 (2019).
37. D. Huber, L. Petreanu, N. Ghitani, S. Ranade, T. Hromádka, Z. Mainen, K. Svoboda, Sparse optical microstimulation in barrel cortex drives learned behaviour in freely moving mice. *Nature* **451**, 61–64 (2008).
38. T. Komiyama, T. R. Sato, D. H. O'Connor, Y.-X. Zhang, D. Huber, B. M. Hooks, M. Gabitto, K. Svoboda, Learning-related fine-scale specificity imaged in motor cortex circuits of behaving mice. *Nature* **464**, 1182–1186 (2010).
39. D. Huber, D. A. Gutnisky, S. Peron, D. H. O'Connor, J. S. Wiegert, L. Tian, T. G. Oertner, L. L. Looger, K. Svoboda, Multiple dynamic representations in the motor cortex during sensorimotor learning. *Nature* **484**, 473–478 (2012).
40. J.-Z. Guo, A. R. Graves, W. W. Guo, J. Zheng, A. Lee, J. Rodríguez-González, N. Li, J. J. Macklin, J. W. Phillips, B. D. Mensh, K. Branson, A. W. Hantman, Cortex commands the performance of skilled movement. *eLife* **4**, e10774 (2015).
41. X. Jin, R. M. Costa, Start/stop signals emerge in nigrostriatal circuits during sequence learning. *Nature* **466**, 457–462 (2010).
42. J. Tanji, Sequential organization of multiple movements: Involvement of cortical motor areas. *Annu. Rev. Neurosci.* **24**, 631–651 (2001).
43. N. Fujii, A. M. Graybiel, Representation of action sequence boundaries by macaque prefrontal cortical neurons. *Science* **301**, 1246–1249 (2003).
44. J. Jia, Z. Puyang, Q. Wang, X. Jin, A. Chen, Dynamic encoding of saccade sequences in primate frontal eye field. *J. Physiol.* **599**, 5061–5084 (2021).
45. A. Nelson, B. Abdelmesih, R. M. Costa, Corticospinal populations broadcast complex motor signals to coordinated spinal and striatal circuits. *Nat. Neurosci.* **24**, 1721–1732 (2021).
46. G. J. Kress, N. Yamawaki, D. L. Wokosin, I. R. Wickersham, G. M. Shepherd, D. J. Surmeier, Convergent cortical innervation of striatal projection neurons. *Nat. Neurosci.* **16**, 665–667 (2013).
47. Y. Mei, P. Monteiro, Y. Zhou, J.-A. Kim, X. Gao, Z. Fu, G. Feng, Adult restoration of Shank3 expression rescues selective autistic-like phenotypes. *Nature* **530**, 481–484 (2016).
48. S. M. Haigh, J. A. Walsh, C. A. Mazefsky, N. J. Minshew, S. M. Eack, Processing speed is impaired in adults with autism spectrum disorder, and relates to social communication abilities. *J. Autism Dev. Disord.* **48**, 2653–2662 (2018).
49. X. Lu, J. Ashe, Anticipatory activity in primary motor cortex codes memorized movement sequences. *Neuron* **45**, 967–973 (2005).
50. A. Sánchez-Fuentes, K. I. Ramírez-Armenta, A. K. Verma-Rodríguez, E. Díaz-Hernández, A. Aguilar-Palomares, J. O. Ramírez-Jarquín, F. Tecuapetla, The contribution of premotor cortico-striatal projections to the execution of serial order sequences. *Eneuro* **8**, ENEURO.0173-21.2021 (2021).
51. H. H. Yin, The role of the murine motor cortex in action duration and order. *Front. Integr. Neurosci.* **3**, 23 (2009).
52. R. Kawai, T. Markman, R. Poddar, R. Ko, A. L. Fantana, A. K. Dhawale, A. R. Kampff, B. P. Ölveczky, Motor cortex is required for learning but not for executing a motor skill. *Neuron* **86**, 800–812 (2015).
53. P. E. Rothwell, S. J. Hayton, G. L. Sun, M. V. Fuccillo, B. K. Lim, R. C. Malenka, Input- and output-specific regulation of serial order performance by corticostriatal circuits. *Neuron* **88**, 345–356 (2015).
54. N. Li, T.-W. Chen, Z. V. Guo, C. R. Gerfen, K. Svoboda, A motor cortex circuit for motor planning and movement. *Nature* **519**, 51–56 (2015).
55. H. B. Simpson, D. S. Vicario, Brain pathways for learned and unlearned vocalizations differ in zebra finches. *J. Neurosci.* **10**, 1541–1556 (1990).
56. J. R. Klug, X. Yan, H. A. Hoffman, M. D. Engelhardt, F. Osakada, E. M. Callaway, X. Jin, Asymmetric cortical projections to striatal direct and indirect pathways distinctly control actions. *eLife 12*, RP92992 (2023).
57. Y. Johansson, G. Silberberg, The functional organization of cortical and thalamic inputs onto five types of striatal neurons is determined by source and target cell identities. *Cell Rep.* **30**, 1178–1194.e3 (2020).
58. M. E. Ragozzino, The contribution of the medial prefrontal cortex, orbitofrontal cortex, and dorsomedial striatum to behavioral flexibility. *Ann. N. Y. Acad. Sci.* **1121**, 355–375 (2007).
59. P. J. Eslinger, L. M. Grattan, Frontal lobe and frontal-striatal substrates for different forms of human cognitive flexibility. *Neuropsychologia* **31**, 17–28 (1993).
60. E. Hoshi, K. Shima, J. Tanji, Task-dependent selectivity of movement-related neuronal activity in the primate prefrontal cortex. *J. Neurophysiol.* **80**, 3392–3397 (1998).
61. E. Hoshi, K. Shima, J. Tanji, Neuronal activity in the primate prefrontal cortex in the process of motor selection based on two behavioral rules. *J. Neurophysiol.* **83**, 2355–2373 (2000).
62. E. Hoshi, J. Tanji, Area-selective neuronal activity in the dorsolateral prefrontal cortex for information retrieval and action planning. *J. Neurophysiol.* **91**, 2707–2722 (2004).
63. H. Mushiake, N. Saito, K. Sakamoto, Y. Itoyama, J. Tanji, Activity in the lateral prefrontal cortex reflects multiple steps of future events in action plans. *Neuron* **50**, 631–641 (2006).
64. K. Nakamura, K. Sakai, O. Hikosaka, Neuronal activity in medial frontal cortex during learning of sequential procedures. *J. Neurophysiol.* **80**, 2671–2687 (1998).
65. A. R. Luria, Two kinds of motor perseveration in massive injury of the frontal lobes. *Brain* **88**, 1–10 (1965).
66. S. D. Iversen, M. Mishkin, Perseverative interference in monkeys following selective lesions of the inferior prefrontal convexity. *Exp. Brain. Res.* **11**, 376–386 (1970).
67. R. Dias, T. Robbins, A. C. Roberts, Dissociable forms of inhibitory control within prefrontal cortex with an analog of the Wisconsin Card Sort Test: Restriction to novel situations and independence from "on-line" processing. *J. Neurosci.* **17**, 9285–9297 (1997).
68. S. Konishi, K. Nakajima, I. Uchida, H. Kikyo, M. Kameyama, Y. Miyashita, Common inhibitory mechanism in human inferior prefrontal cortex revealed by event-related functional MRI. *Brain* **122**, 981–991 (1999).
69. A. R. Aron, P. C. Fletcher, E. T. Bullmore, B. J. Sahakian, T. W. Robbins, Stop-signal inhibition disrupted by damage to right inferior frontal gyrus in humans. *Nat. Neurosci.* **6**, 115–116 (2003).
70. Y. Agam, R. M. Joseph, J. J. Barton, D. S. Manoach, Reduced cognitive control of response inhibition by the anterior cingulate cortex in autism spectrum disorders. *Neuroimage* **52**, 336–347 (2010).
71. S. E. Ahmari, T. Spellman, N. L. Douglass, M. A. Kheirbek, H. B. Simpson, K. Deisseroth, J. A. Gordon, R. Hen, Repeated cortico-striatal stimulation generates persistent OCD-like behavior. *Science* **340**, 1234–1239 (2013).
72. E. Burguière, P. Monteiro, G. Feng, A. M. Graybiel, Optogenetic stimulation of lateral orbitofronto-striatal pathway suppresses compulsive behaviors. *Science* **340**, 1243–1246 (2013).
73. E. E. Manning, A. Y. Dombrovski, M. M. Torregrossa, S. E. Ahmari, Impaired instrumental reversal learning is associated with increased medial prefrontal cortex activity in Sapap3 knockout mouse model of compulsive behavior. *Neuropsychopharmacology* **44**, 1494–1504 (2019).
74. B. Guo, J. Chen, Q. Chen, K. Ren, D. Feng, H. Mao, H. Yao, J. Yang, H. Liu, F. Jia, C. Qi, T. Lynn-Jones, H. Hu, Z. Fu, G. Feng, W. Wang, S. Wu, Anterior cingulate cortex dysfunction underlies social deficits in Shank3 mutant mice. *Nat. Neurosci.* **22**, 1223–1234 (2019).
75. A. M. Graybiel, S. L. Rauch, Toward a neurobiology of obsessive-compulsive disorder. *Neuron* **28**, 343–347 (2000).
76. H. H. Yin, B. J. Knowlton, B. W. Balleine, Blockade of NMDA receptors in the dorsomedial striatum prevents action-outcome learning in instrumental conditioning. *Eur. J. Neurosci.* **22**, 505–512 (2005).
77. H. H. Yin, B. J. Knowlton, B. W. Balleine, Lesions of dorsolateral striatum preserve outcome expectancy but disrupt habit formation in instrumental learning. *Eur. J. Neurosci.* **19**, 181–189 (2004).

Acknowledgments: We would like to thank G. Feng and W. Wang for the *Shank3* $^{fx/fx}$ mice and H. Li, A. Sho, and members of X.J.'s laboratory for discussion and comments on the manuscript. **Funding:** This research was supported by the China Postdoctoral Science Foundation (2023 M741185), the Hewitt Foundation Fellowship, the NIH grant R01NS083815, and the McKnight Memory and Cognitive Disorders Award. X.J. is a New Cornerstone Investigator. **Author contributions:** Conceptualization: X.J. and B.Z. Methodology: X.J., B.Z. and C.E.G. Software: B.Z. Validation: X.J. and B.Z. Formal analysis: B.Z. Investigation: B.Z. and C.E.G. Resources: X.J. Data curation: X.J. and B.Z. Writing–original draft: X.J. and B.Z. Writing–review and editing: X.J. and B.Z. Visualization: B.Z. Supervision: X.J. Project administration: X.J. and B.Z. Funding acquisition: X.J. and B.Z. **Competing interests:** The authors declare that they have no competing interests. **Data and materials availability:** All data needed to evaluate the conclusions in the paper are present in the paper and/or the Supplementary Materials.

Submitted 12 September 2024
Accepted 18 April 2025
Published 23 May 2025
10.1126/sciadv.adt0854